Two-Colour Nonlinear Amplification for Mid-infrared Generation by Difference Frequency Generation

by

Samuel Laketa

A thesis
presented to the University of Waterloo
in fulfillment of the
thesis requirement for the degree of
Master of Science
in
Physics

Waterloo, Ontario, Canada, 2024

Author's Declaration

I hereby declare that I am the sole author of this thesis. This is a true copy of the thesis, including any required final revisions, as accepted by my examiners.

I understand that my thesis may be made electronically available to the public.

Abstract

In this thesis, I discuss the development of a two-colour laser system which uses an all-normal dispersion fiber laser in combination with a gain-managed nonlinear amplifier as its broadband source. The goal is to develop a two-colour laser which can be used for mid-infrared generation through difference frequency generation. Most molecules contain characteristic absorption features in the mid-infrared "molecular fingerprint" region from 3 - 20 μm. Our goal is to create a high power laser that can access as much of these wavelengths as possible. This requires a wide wavelength separation between colours, along with broad bandwidths in each colour, while attaining high pulse energies. This work shows the use of nonlinear amplification of a two-colour seed in an Yb:fiber in order to combat gain narrowing and maintain broad wavelengths in the two colours through self-phase modulation. Many different experimental setups were implemented, which will be presented, with the most successful results being achieved with the use of a large-mode-area Yb:fiber. We demonstrate a two-colour laser source with colours centered at 1070 nm and 1120 nm with individual bandwidths of 30 nm and 21 nm respectively. This two-colour spectrum was amplified up to a total power of 6.76 W, with a repetition rate of 9.67 MHz, corresponding to a total pulse energy of 700 nJ.

Acknowledgements

First and foremost, I would like to thank my supervisor, Professor Donna Strickland, for her guidance and mentorship. Her willingness to share her expertise through insightful discussions has been invaluable throughout my master's degree.

I would also like to thank Mingjian Peter Lyu and Dean Eaton for passing down their knowledge to me from the first day that I joined this research team. I am deeply thankful for the teamwork, support, and conversations throughout the entirety of my research.

Lastly, I would like to thank Professors Joseph Sanderson and German Sciaini for serving on my advisory committee and setting time apart to provide me with feedback and suggestions.

Dedication

This is dedicated to my family as a small token of appreciation for their steadfast dedication and unwavering support for me.

Table of Contents

List of Figures

Chapter 1

Introduction

This thesis focuses on the development of a two-colour laser system which can be used for mid-infrared (MIR) generation through difference frequency generation (DFG). It will discuss the implementation of an ultrafast laser system, comprising of an all-normal dispersion (ANDi) fiber laser and a gain-managed nonlinear amplifier (GMNA), as a broadband source from which we can select two-colours. The methods of selection and nonlinear amplification of these two colours is then discussed.

The goal with this research was to achieve a short pulse two-colour laser with as broad a separation between colours as possible and a broad bandwidth in each colour, all while amplifying to the Watt level. The motivation for this being the development of a source which could be used for difference frequency generation in a nonlinear crystal to produce tunable, short pulse mid-infrared radiation. The overall goal with this research is to generate MIR that is tunable across as much of the "molecular fingerprint" region as possible. The molecular fingerprint region refers to the wavelengths ranging from 3 - 20 μm where many molecules contain strong, characteristic absorption features [2]. Broadband ultrashort MIR sources find application in gas detection [3], pollutant monitoring [4], cancer diagnosis [5], and even food quality control [6]. These sources notably find defense appli-

cations as well since many explosive materials show clear signatures within the molecular fingerprint region [7], allowing for remote detection using MIR spectroscopy.

Ultrashort two-colour lasers have previously been developed using Yb:fiber lasers or Ti:sapphire lasers. Many of these two-colour systems were developed for MIR generation through difference frequency generation. This is commonly performed in a GaSe crystal due to its high nonlinearity and transparency at wavelengths above 10 μm. The transparency of GaSe is limited at 20 μm, which corresponds to difference frequency mixing wavelengths that are approximately 55 nm apart, necessitating two-colour lasers with at least this wavelength separation.

A drawback of the two-colour lasers previously reported is the gain narrowing that occurs with each colour. This limits their bandwidth, which then limits the overall tunability of generated MIR as well as the pulse duration. In this work, we take advantage of nonlinear effects to try and combat gain narrowing. Based on the work by Sidorenko et al. [8], we seed an Yb:amplifier with a two-colour spectrum at a ps-level pulse duration with the goal of compensating for the gain narrowing and further broadening our two-colours, while simultaneously amplifying them. In this research, we achieved a two-colour laser with colours centered at 1070 nm and 1120 nm, corresponding to a wavelength separation of 50 nm. Although this is less than the desired threshold of 55 nm separation, which is determined by the transparency of GaSe crystals, the bandwidths of each colour were improved. The lower wavelength blue colour displayed broadening, with a resulting bandwidth of 30 nm and the red colour maintained a bandwidth of 21 nm. If we consider the inner and outermost wavelengths, this corresponds to wavelength separations from 25 - 80 nm. The two-colour spectrum was amplified up to 6.76 W with a total pulse energy of 700 nJ.

Chapter 2 of this thesis will discuss the necessary background information required to understand our experimental setup, including ytterbium-doped fiber amplifiers, all-normal dispersion fiber lasers, gain-managed nonlinear amplification as well as the most relevant nonlinear effects. Chapter 3 will then provide a background and literature review

on the systems used for generating short-pulse mid-infrared. Chapter 4 will discuss our experimental setup and results, including the implementation of the ANDi and GMNA as our ultrafast broadband source, and the various experimental setups utilized for two-colour selection and amplification. The conclusion will then be presented in chapter 5.

Chapter 2

Background

2.1 Fiber Amplifier Fundamentals

The phenomenon of total internal reflection acts as the guiding mechanism for light in optical fibers. The basic configuration of optical fibers includes the concentric core and cladding, the latter of which has a lower index of refraction. This enables light to undergo total internal reflection in the core and travel throughout the fiber.

Doped fiber amplifiers allow one to amplify the power of a desired seed signal by optically pumping a rare-earth ion doped fiber. The essential operating principle consists of shorter wavelength pump light being launched into a fiber where the rare-earth ions can absorb the photons, exciting them into metastable states. Longer wavelength signal light can then be amplified through stimulated emission from these excited ions.

The excited states do have an effective lifetime as the ions spontaneously de-excite, effectively lowering their energy. This process produces a photon which can then propagate throughout the fiber and be amplified through stimulated emission. This phenomenon is referred to as amplified spontaneous emission (ASE) and acts as noise in a fiber amplifier

as well as limiting the availability of excited electrons to be used for the amplification of the seed signal.

High output power doped fiber amplifiers utilize double-clad fibers which consist of a doped, single-mode core, in which the seed signal is to be coupled into, surrounded by an undoped multi-mode inner cladding where high-power pump light may be launched. The inner cladding is surrounded by an outer cladding which has a lower index of refraction, effectively confining the pump to the inner cladding. As the pump light propagates throughout the cladding, it passes through the core, effectively exciting the rare-earth dopants through absorption.

2.2 Ytterbium Doped Fiber Amplifiers

Lasing in ytterbium-doped silicate glass was demonstrated in 1962 by Etzel et al. [9]. It was not until 1988 that lasing was demonstrated in an ytterbium-doped silica fiber where Hanna et al. [10] used an 840 nm dye laser to pump the Yb-doped fiber and achieved tunability from 1015 – 1140 nm. This broad tunability is due to the fact that YDFAs exhibit a homogenous emission spectrum from 900 – 1200 nm [1]. Its maximum emission occurs at 975 nm with a second maximum at 1030 nm. The absorption spectrum also peaks at 975 nm with a second maximum at 910 nm, as seen in figure 2.1. It spans from about 850 – 1100 nm, making YDFAs accessible to a wide range of pump wavelengths.

Taking advantage of the peak absorption at 975 nm results in over 200 nm of potential gain. According to Fourier transform theory, a broad bandwidth in frequency space corresponds to a short pulse duration, making Ytterbium-doped fiber lasers an ideal candidate for generating ultrashort pulsed lasers. Mode-locked Ytterbium fiber lasers have been used to generate 33 fs pulses [11], 28.3 fs pulses [12], and sub-25 fs pulses [13]. Kurita et al [14] achieved 21.6 fs pulses by pumping at 915 nm, instead of the common wavelength of 975 nm, yielding a broad spectrum spanning 950 – 1090 nm.

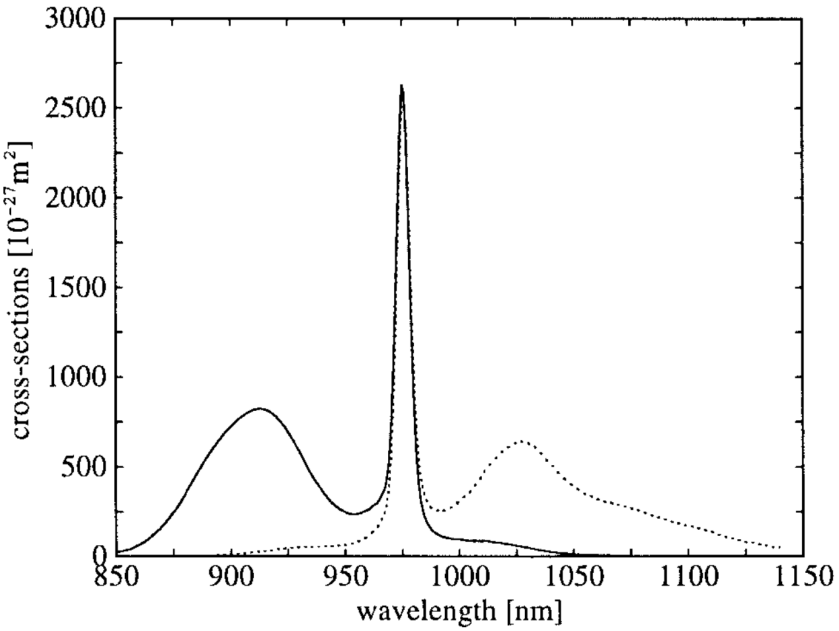

Figure 2.1: Absorption and emission cross sections (solid and dotted respectively) of Yb-doped glass. Figure from Paschotta et al. [1]

Ytterbium fiber lasers also have the capability of delivering high power lasers. YDFA-based systems have been used to achieve high average output powers of 10.4 kW with sub-300 fs pulses at an 80 MHz repetition rate [15]. Higher pulse energies of 10 mJ were reached by Stark et al [16] with a corresponding average output power of 1 kW with a 120 fs pulse duration. Additionally, continuous-wave (CW) Yb-fiber lasers have reached ultra-high output powers of over 100 kW [17, 18].

Yb-fiber lasers have been able to achieve such high output powers due to multiple properties [19, 20]. Firstly, fiber lasers contain a low surface-to-volume ratio allowing for excellent heat dissipation. Ytterbium-doped silica specifically also has a low quantum defect of less than 10%, defined as the energy difference between the pump and signal photons, allowing for optical-to-optical efficiencies above 80% and mitigating thermal load on the system. Additionally, rare-earth-doped fibers have low intrinsic losses, typically less

than 10 dB/km, allowing for longer fiber lengths to be used and furthering the efficiency of Yb-fiber laser systems. Finally, double-clad pumping utilizes the inner cladding as the waveguide for high-power, multi-mode laser diode pumps, pushing power limits well past the few-Watt output limit of single-clad designs.

2.2.1 Two-Colour Yb:fiber Amplifiers

Ultrashort two-colour lasers have previously been developed with wavelength separations at or above 60 nm. Liu et al. [21] utilized a photonic crystal fiber to generate a supercontinuum spectrum from which they selected two colours with 60-nm wavelength separation. After amplification in an Yb:fiber amplifier, they reported a total power of 450 mW. Romero-Alvarez et al. [22] improved upon this setup to yield a 65 nm wavelength separation with colours centered at 1038 nm and 1103 nm and an average power of 300 mW. Al-Kadry and Strickland [23] incorporated the chirped pulse amplification (CPA) technique in their two-colour ultrafast Yb:fiber laser. They reported a 67 nm wavelength separation with a total power of 1.1 W after amplification. More recently, Strickland's ultrafast laser team moved from using mainly bulk-optic elements to a partially fiberized system [24]. The system consisted of a high-power, fiber-coupled CPA system which utilized a chirped fiber Bragg grating to filter out a 60 nm notch from a spectral continuum, resulting in two colors centered at 1025 and 1085 nm with a total average power of 2.3 W. These two-colour systems were developed for MIR generation through difference frequency generation.

Budz et al. utilized two electronically synchronized mode-locked external-cavity semiconductor oscillators and a single Yb-doped fiber amplifier to yield a dual-wavelength source [25]. The synchronized oscillators operated at wavelengths of 1040 nm and 1079 nm, corresponding to amplified pulses with 39 nm of separation and a total average power of 1.1 W. Two-colour passively modelocked Yb:fiber lasers have been reported as well. Bai et al. [26] demonstrated a passively modelocked dual-wavelength fiber laser based on

semiconductor saturable absorber mirror (SESAM) which had a maximum wavelength separation of 35 nm and pulse energies of 0.47 nJ and 0.33 nJ in the respective colours. More recently, Zhu et al. reported a dual wavelength Yb:doped all-normal dispersion (ANDi) fiber laser [27]. A Sagnac loop is used as the spectrum filter for dual-wavelength tuning which is adjusted through a polarization controller. The multi-wavelength modelocked output could be tuned with up to 50 nm of wavelength separation between the two colours. The average powers of each colour were 42.3 mW and 11 mW, corresponding to pulse energies of 18.5 nJ and 4.8 nJ respectively.

Although Ytterbium-doped fiber amplifiers provide up to 210 nm of potential gain, achieving a large wavelength separation in a two-colour Yb:fiber laser that takes advantage of this full bandwidth is difficult due to the gain competition at different wavelengths. The lower gain at the longer wavelengths are suppressed by the shorter wavelengths which are closer to the gain peak at 1030 nm. This proves to be a challenge for increasing the wavelength separation between colours to the level attainable by Ti:sapphire lasers.

2.3 Ti:Sapphire Two-Colour Lasers

The main competitor to Yb:fiber amplifiers in the two-colour laser space is the Ti:sapphire laser. This is largely due to its broad gain bandwidth which spans from 670-1070 nm and peaks at around 800 nm [28]. The broad absorption band peaks around 490 nm with a bandwidth of $\sim$200 nm and so green argon lasers are often used to pump Ti:sapphire lasers, or frequency doubled Nd:YAG lasers [28, 29]. This large gain bandwidth has enabled two-colour ultrafast lasers to be built using the output of a single Ti:sapphire oscillator.

Evans et al. [30] pumped a Ti:sapphire rod using a single argon laser beam while incorporating a dual cavity setup to yield a dual-wavelength oscillator with individually tunable colours centered at 760 nm and 850 nm. Simultaneous modelocking was achieved through cross phase modulation. The two colours, with output powers of 150 mW each,

could be tuned individually through 3 intracavity prisms. Similarly, Leitenstorfer et al. [31] used a single argon laser to pump a Ti:sapphire rod in a dual X-folded cavity configuration with synchronization achieved through cross phase modelocking. The prism compressors and output couplers could be adjusted separately for each colour, providing independant tunability. They achieved wavelength separations as wide as 100 nm with individual colour output powers of up to 500 mW.

Donna Strickland's ultrafast laser team demonstrated two-colour ultrafast Ti:sapphire chirped pulse amplifiers which were seeded by a dual-wavelength Ti:sapphire oscillator [32, 33]. Zhang et al. [32] utilized a dual cavity system around a Ti:sapphire crystal which was pumped by an argon laser. Their chirped-pulse amplification system simultaneously amplified the two-colour oscillator in a regenerative amplifier after stretching the pulses using a single grating. The gain medium of the regenerative amplifier was a Ti:sapphire rod. After compression of the pulses, they achieved a total energy of 1.5 mJ between the two colours which could be tuned from 800 to 890 nm. The same setup was used by Xia et al. [33], but they included a regenerative amplifier in combination with a Ti:sapphire multi-pass amplifier which allowed them to reach a total pulse energy of 15 mJ after compression. The two colours were tunable between 800 and 890 nm. Fraser et al. demonstrated a dual wavelength Ti:sapphire amplifier which was seeded by a spectrally-shaped injection beam from a single Ti:sapphire oscillator [34]. Spectral shaping was performed in the pulse stretcher by placing an opaque card in the Fourier plane of the injection beam and then making the desired adjustments based on the observed amplifier output. The two-colour pulses were then passed through a regenerative amplifier system. Upon compression, they achieved a total pulse energy of $\sim$1 mJ with wavelength separations up to 55 nm centered at 820 nm. Yamakawa and Barty also utilized a spectrally shaped single Ti:sapphire oscillator for their two-colour chirped pulse amplifier [35]. Upon amplifying pulses centered at 740 and 861 nm in a regenerative amplifier, they achieved pulse energies of up to 5 mJ in each colour with central wavelength separations of 120 nm.

The power of Ti:sapphire laser amplifiers are limited by the power of their green pump

lasers due to thermal lensing. With green lasers operating around 532 nm, and Ti:sapphire lasing occurring around 800 nm, the large quantum defect inevitably generates significant amounts of heat in the crystal. The temperature gradient that occurs acts as a lens in the crystal, which can eventually damage the crystal. Thermal lensing occurs in Ti:sapphire crystals at the threshold of ∼7-W of average pump power [36] while at room temperature. Cooling techniques must then be used in order to increase the pump power thermal lensing limit. While limited in power, Ti:sapphire provides a broader gain bandwidth with which to generate two-colour lasers from when compared to Yb:doped fibers, resulting in larger wavelength separations. Ytterbium-doped fiber amplifiers, on the other hand, provide a more compact solution for a two-colour laser with higher power potential, albeit with a more narrow gain bandwidth. Additionally, Yb:fiber lasers have the advantage over Ti:sapphire lasers when it comes to avoiding two-photon absorption (TPA) while difference frequency mixing pump and signal photons in a nonlinear crystal. Since the absorption edge for nonlinear crystals is often around 0.5 μm, the incident wavelengths should be above 1 μm to avoid TPA. Yb:fiber lasers have the advantage in this regard since the gain region is above this TPA-imposed cut-off wavelength.

2.4 Nonlinear Optics

When electromagnetic fields are sufficiently intense, they can induce changes in the optical properties of a material system, such as an optical fiber. This results in various nonlinear optical phenomena occurring [37, 38, 39] which can be used to one's advantage in controlling the properties of output pulses in laser systems. In linear optics, the induced polarization of a material system can be described as $\tilde{P}(t) = \epsilon_0 \chi^{(1)} \tilde{E}(t)$ while in nonlinear optics the polarization is expressed as a power series in the electric field as

$$\tilde{P}(t) = \epsilon_0 [\chi^{(1)} \tilde{E}(t) + \chi^{(2)} \tilde{E}^2(t) + \chi^{(3)} \tilde{E}^3(t)] + ...] \tag{2.1}$$

where $\chi^{(1)}$ represents the linear susceptibility and $\chi^{(2)}$ and $\chi^{(3)}$ represent the second and third order nonlinear optical susceptibilities respectively. The permittivity of free space is

represented by ϵ_0.

The second order nonlinear susceptibility is responsible for nonlinear effects such as difference frequency generation and second-harmonic generation, but $\chi^{(2)}$ is only non-zero for materials that lack inversion symmetry. Since silica-based based fibers are composed of the symmetric molecule SiO_2, these second-order nonlinear processes do not manifest. Most nonlinear effects that occur in optical fibers are due to the third order $\chi^{(3)}$ phenomena of nonlinear refraction.

2.4.1 Self-Phase Modulation

Nonlinear refraction refers to the intensity dependence of the refractive index, also known as the optical Kerr effect, described by

$$n(I) = n + n_2 I \tag{2.2}$$

where n and n_2 correspond to the refractive index and nonlinear refractive index respectively, and I represents the intensity. During propagation through an optical fiber of length L, an optical field will experience a phase change given by

$$\phi(t) = -kn(I)L = -kL\left[n + n_2 I(t)\right] \tag{2.3}$$

where $k = 2\pi/\lambda$. The intensity-dependant nonlinear phase shift is then given by

$$\phi_{NL}(t) = -n_2 kLI(t) = -n_2 kL\left|A(t)\right|^2 \tag{2.4}$$

where $\left|A(t)\right|^2$ is the amplitude of the optical field's pulse envelope inside the fiber.

The nonlinear phase shift ϕ_{NL} is due to self-phase modulation (SPM). SPM primarily broadens the spectrum of an optical pulse while leaving the pulse shape in time unchanged.

This can be understood by the time-dependence of the nonlinear phase shift, which implies that the instantaneous frequency differs across the pulse from its central wavelength. This change in instantaneous frequency is given by

$$\delta\omega(t) = \frac{d\phi_{NL}}{dt} = -n_2 k L \frac{dI(t)}{dt} \tag{2.5}$$

from which we can interpret the effects of self-phase modulation. The leading edge of the pulse corresponds to a positive dI/dt which then leads to a reduction in frequency, or a red shift. The trailing edge corresponds to a negative dI/dt and therefore an increase in frequency or a blue shift. This frequency chirping, induced by SPM, continues as the pulse propagates down the fiber, continuously creating new frequency components and broadening the spectrum. The amount of broadening is understandably dependent on the slope of the leading and trailing edge of the pulse, with steeper edges corresponding to larger frequency chirping.

SPM-induced spectral broadening exhibits an oscillatory structure across the entire frequency range with characteristically more intense peaks on the edges of the spectrum. These oscillations can be qualitatively explained to be generated by the interference between waves of the same instantaneous frequency but with different phases, leading to either constructive or destructive intereference.

2.4.2 Raman Scattering

Raman scattering is a third-order nonlinear process which involves the interaction of photons and phonons to generate frequencies that are higher and lower than the excitation source. One can consider the quantum energy levels of figure 2.2 to describe the process that occurs after light is incident on a Raman active material. Light with frequency ω interacts with the material and can excite the electron up from the ground state to a virtual state, $|v_1\rangle$. If this electron goes through de-excitation down to $|e\rangle$, a stokes photon

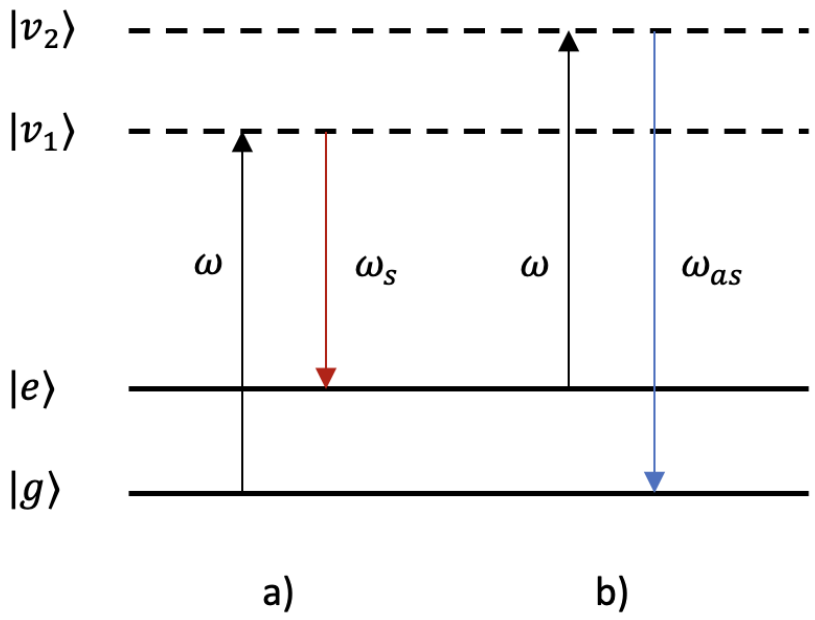

Figure 2.2: Energy level diagram for the generation of a a) stokes photon and an b) anti-stokes photon

is released at a frequency of ω_s which is lower than that of the incident frequency. The remaining energy is absorbed in a molecular vibrational state with energy $\omega - \omega_s$.

If the molecule is already in an excited state $|e\rangle$, due to molecular vibrations for example, then the excitation photon of frequency ω can get absorbed into the virtual state $|v_2\rangle$. From here, a de-excitation down to the ground state is possible which would create an anti-stokes photon with a higher energy than the incident light. This is caused by the additional energy gained from the vibrational energy of the molecule. An electron populating the excited state is also made possible from the generation of a stokes photon, as we have just mentioned, allowing the initial excitation into the $|v_2\rangle$ state before the creation of an anti-stokes photon.

2.4.3 Dispersion

Chromatic dispersion is a result of the frequency dependence of the refractive index $n(\omega)$. This manifests in different frequencies of light propagating at different velocities through the transmitting medium, which ultimately leads to an increase in pulse duration. Understanding and controlling the dispersion of a pulse is critical for ultrafast lasers as it will directly influence the pulse duration and intensity of the pulses.

Ultrashort pulses propagating through fibers will undergo dispersion as each frequency component travels at a speed given by $v = c/n(\omega)$. The effects of dispersion are often described through a Taylor expansion of the propagation constant β around the center frequency ω_0, given by

$$\beta(\omega) = n(\omega)\frac{\omega}{c} = \beta_0 + \beta_1(\omega - \omega_0) + \frac{1}{2}\beta_2(\omega - \omega_0)^2 + ... \tag{2.6}$$

where we have only expanded to the third order as this will generally include all necessary dispersive effects. Here,

$$\beta_n = \left(\frac{d^n\beta}{d\omega^n}\right)_{\omega=\omega_0} \tag{2.7}$$

where $n = 0, 1, 2$.

An ultrashort pulse's carrier envelope will travel at the group velocity, which is given by the inverse of β_1. The dispersion of the group velocity is described by β_2. This parameter is ultimately responsible for pulse broadening and is known as the group velocity dispersion (GVD) parameter. Since ultrashort pulses contain broad bandwidths, and GVD is highly wavelength dependent, ultrashort pulses are strongly affected by dispersion and pulse broadening.

The sign of the GVD parameter β_2 is important to note. If $\beta_2 > 0$, then the lower frequency components of the pulse travel faster than the higher frequency components. This is known as normal dispersion. When $\beta_2 < 0$, the lower frequency components travel slower than the higher frequency components of the pulse, which is known as the anomalous

dispersion regime. The sign of β_2 switches from positive to negative at the zero-dispersion wavelength at which β_2 actually vanishes. It is at this point that the effects of third-order dispersion must be accounted for, described by the β_3 coefficient.

2.5 Gain-Managed Nonlinear Amplification

Ultrafast fiber lasers serve as a compact solution for delivering high-power pulses with excellent thermal management and beam quality. As peak powers are increased in fiber laser systems, the accumulation of non-linear effects, such as self-phase modulation, stimulated Raman scattering and self-focusing, becomes prevalent. Chirped pulse amplification (CPA) [40] systems are commonly incorporated to remove unwanted non-linear effects by stretching the input pulses before amplifying, resulting in lower peak intensities during propagation in the fiber. The output pulses are subsequently compressed, yielding high-power ultrafast pulses.

These CPA systems are limited to pulse durations of about 200 fs due to gain narrowing [41]. Gain narrowing occurs under amplification as the higher power central wavelengths of an optical spectrum experience more gain than the outer wings of the spectrum, leading to a narrowing of the bandwidth. Nonlinear amplification systems have been used to realise pulses with durations below this limit through methods such as direct amplification [42], pre-chirp management [43], and self-similar pulse evolution [44]. Self-similar pulse evolution is relatively insensitive to the input pulse parameters as it utilizes a non-linear attractor, while pre-chirp management requires fine tuning of the seed characteristics, further increasing the complexity of the system. Self-similar pulse evolution suffers from the fact that the optical spectrum of an amplified pulse can exceed the gain bandwidth at higher powers, resulting in distortions of the chirp and frequency envelope [45]. This leads to degradation in pulse compression efficiency.

Sidorenko et al. demonstrated a novel method of nonlinear amplification referred to as

gain-managed nonlinear amplification (GMNA) [46]. In a gain-managed nonlinear amplifier, the seeded narrowband (1-5 nm) pulse undergoes up to 100-fold spectral broadening while maintaining compressibility down to the transform-limited duration using a simple grating compressor. This approach takes advantage of nonlinear effects to broaden the spectrum while simultaneously being balanced by gain-shaping. The gain and pulse spectra reshape one another in tandem during amplification, giving rise to the name of the gain-managed nonlinear (GMN) regime. A key advantage to this approach to nonlinear amplification is a linearly chirped output pulse, resulting in the ability to cleanly compress pulses after undergoing significant nonlinear spectral broadening. In their first demonstration of the GMN regime, they used a 3 m Yb-doped fiber amplifier seeded by 1.7 nm pulses with 3 nJ of energy. The GMNA yielded 100 nm bandwidth pulses which could be compressed down to 39 fs with an energy of 77 nJ. It was found that gain-managed nonlinear amplification was driven by a nonlinear attractor, making it relatively insensitive to the seed input, similar to self-similar pulse evolution.

A follow-up paper was released which further expanded on the mechanisms involved in the pulse evolution during the GMN regime and its limitations [8]. The GMN (gain-managed non-linear) regime can be defined as the process of non-linear spectral broadening being balanced by gain-shaping, manifesting as absorption of the blue side of the spectrum and amplification of the red. They simulated launching 1 ps Gaussian pulses centered at 1028 nm into a 5-m Yb-doped fiber amplifier with 6-um diameter core, while co-pumping at 976 nm. The initial pulse evolution is shown to be dominated by self-phase modulation, symmetrically broadening the spectrum until the blue side is limited by the absorption around 1020 nm. The red side of the spectrum continues to broaden as the gain curve shifts towards the red. After about 2 m, temporal broadening due to dispersion overcomes the gain, consequently decreasing the peak power. As gain and peak power begin to decrease further along the fiber, the spectral broadening stops with the blue side limited by absorption and the red side limited by the waning gain. The pulse evolves to have an asymmetric time-domain profile with a smooth spectrum as its pulse energy increases and obtains a nearly linear chirp that can be compensated for by a simple grating pair. This

allows one to compress down to near Fourier-transform limited pulses.

An experimental demonstration was performed using a 5-m Yb-doped fiber amplifier with a 5-um core diameter seeded with 700 fs, 1 nJ pulses. They achieved substantial broadening with the spectrum extending past 1100 nm and overflowing the gain bandwidth of the Yb-doped fiber. As pump powers were increased, shot-noise seeded Raman scattering was observed, manifesting as a small spectral-shoulder on the red edge of the spectrum. This stimulated Raman scattering serves as the limit for pulse energies obtained through GMNA. At the highest amplified pulse energy of 107 nJ, a grating pair was used to compress the pulses down to 42 fs.

Frank Wise's group continued their research by investigating the energy scaling potential of GMNA in a large-mode-area (LMA) gain fiber [47]. The GMN amplifier was seeded with 1 nJ pulses centered at 1025 nm with a 0.6 ps pulse duration. The LMA gain fiber consisted of a 30 um core diameter and 400 um cladding diameter. The 3-m Yb gain fiber was co-pumped with a 976-nm 60 W diode. The seed pulse was amplified up to 1.2 uJ with an average power of 6.5 W and a pulse duration of 38 fs, with the maximum pulse energy being limited by stimulated Raman scattering once again. This served as a significant increase in the performance of GMN amplifiers, while maintaining their simplicity.

2.6 All-Normal Dispersion Fiber Laser

An all-normal dispersion (ANDi) fiber laser provides a compact solution for generating relatively high-energy, ultrashort pulses through passive modelocking. Ultrashort pulses are commonly obtained under the anomalous dispersion regime where the GVD and SPM balance each other to produce soliton pulses. By utilizing an all-normal dispersion fiber laser, dispersion controls that introduce losses in the cavity, such as prisms, gratings, and chirped mirrors, do not have to be implemented. These fiber lasers produce highly chirped picosecond pulses that can be compressed outside of the laser to femtosecond levels.

2.6.1 Basics of Modelocked lasers

Modelocking is a method used for generating ultrashort pulses from lasers [39],[48]. A modelocked laser emits a train of pulses with a period given by the length of the cavity divided by the group velocity of the pulse, which for a linear cavity would include a factor of 2 to account for the round trip, $T = 2L/v_g$. This corresponds to a repetition rate in the frequency domain given by $f_{rep} = v_g/2L$. Modelocking can be categorized into active and passive techniques. Active-modelocking involves external intervention to control the parameters of the resonant cavity through an electronically driven periodic signal. Passive modelocking utilizes a saturable absorber within the laser cavity to generate modelocking.

Due to their nonlinear characteristics, saturable absorbers contain high absorption for low intensity light, and low absorption for high optical intensities. They can be grouped into artificial and real saturable absorbers. Real saturable absorbers are based on the nonlinear effects of the object's material itself that enable it to act as a saturable absorber, while artificial saturable absorbers are based on the nonlinear effects of the fiber but are not necessarily absorbers. They do, however, provide higher transmission for higher optical intensities in various other ways. Passive modelocking is initiated by noise spikes in the laser which, when strong enough, pass through the saturable absorber with lower absorption and can then be further amplified by the gain medium. This results in less loss through the saturable absorber with every subsequent roundtrip of the cavity until a pulse train in the steady state is formed.

2.6.2 Nonlinear Polarization Evolution Modelocking

A popular method of passive modelocking, which is utilized in an all-normal dispersion fiber laser, is nonlinear polarization evolution [49]. This method utilizes the evolving polarization states in a fiber in combination with polarization controllers to act as an artificial saturable absorber.

An elliptical polarization state can evolve in a fiber as a nonlinear response to a high-intensity pulse. This is due to a combination of the birefringence of fibers and self-phase modulation. By introducing waveplates and a polarizing beam splitter, the polarization can be adjusted such that the polarization with the highest optical intensity experiences the lowest loss. This setup then acts as an artificial saturable absorber and can be used to passively mode-lock the laser.

The starting of such a laser is initiated through quantum noise [50],[39]. A random, intense fluctuation will initiate the process of a signal achieving lower losses through the artificial saturable absorber which can then turn into a pulsed signal that can be amplified with each round trip. This is generally insufficient to create a stable mode-locking state, and so additional pulse shaping is necessary.

Spectral filtering aids in the robustness of the generated ultrashort pulses under the normal GVD regime. By selecting an appropriate filter bandwidth, one can select desired modes while attenuating others that would otherwise be permitted by the gain bandwidth. This has a non-trivial effect on the mode-locked pulse's chirp, amplitude, and width. Bale et al. [51] found that engineering the laser cavity with an appropriate filter bandwidth, along with an optimal distance between the filter and output coupler, led to robust, high-energy, ultrafast pulses in the normal GVD regime.

Spectral filtering can be achieved through the use of a bandpass filter, which is used to transmit a specified set of wavelengths while rejecting others. Bandpass filters lack in flexibility as the transmitted bandwidth and center wavelength are generally fixed with some angle-sensitive adjustments available. Utilizing a dispersion grating as a spectral filter allows for more customization. By placing a grating before a fiber, one can control the spectral bandwidth inputted into the fiber by adjusting the distance between the fiber and grating. The center wavelength of the spectral filter can then be controlled by adjusting the angle of the dispersion grating.

2.6.3 ANDi Components and Design

Ultrafast lasers will often have segments of normal and anomalous group-velocity dispersion. When the net dispersion is anomalous, self-phase modulation can balance dispersion to generate short soliton pulses with little chirp. Higher energy pulses can be attained with more normal dispersion in the laser, which served as the motivation for the development of the all-normal dispersion (ANDi) fiber laser [52]. Chong et al. simulated and demonstrated a femtosecond fiber laser which consisted of only normal GVD within the cavity. This meant that all dispersion control components inside the cavity could be removed, such as gratings and prisms, which would introduce losses. The ANDi would produce highly chirped picosecond pulses that could be externally compressed down to the femtosecond level by a pair of dispersion gratings.

The ANDi consists of four main elements which include a long segment of single-mode fiber, a short segment of gain fiber, followed by a shorter segment of single-mode fiber and nonlinear polarization evolution (NPE) components whose ejection port serves as the laser output. Additionally, a spectral filter is included in the cavity in order to establish a stable modelocking state. It was found that the gain bandwidth played a significant role how the pulse evolved in the cavity. When the bandwidth was large ($\sim$30 nm) the pulses evolved like that of a self-similar laser, while pulses with bandwidths below 10 nm did not provide solutions that converged. At bandwidths around 10 nm, the spectrum developed sharp peaks on its edges, indicative of self-phase modulation and serving as the characteristic spectrum of a stable modelocking state in an ANDi.

An Yb-doped fiber was used as the gain fiber, pumped by a 980-nm laser diode allowing strong amplification of wavelengths around 1030 nm. The passive-mode locking technique of NPE was implemented using quarter-wave plates, half-wave plates and a polarizing beamsplitter (PBS). Spectral filtering was accomplished by a bandpass filter centered at 1030 nm with a 10-nm bandwidth. By controlling the length of the single-mode fibers in the cavity, one could vary the repetition rate of the laser by varying the distance that light

travels in the cavity.

The laser produced highly chirped 1.4 ps pulses that could be compressed down to 170 fs with a pair of diffraction gratings. The output pulses had an energy of 2.7 nJ. Chong et al. made adjustments to the cavity parameters and succesfully demonstrated stable 20-nJ pulses from an ANDi only a year later [53].

2.7 Chirped Pulse Amplification

Chirped pulse amplification (CPA) was developed by Strickland and Mourou in 1985 [40] as a technique for amplifying ultrashort pulses while avoiding unwanted nonlinear effects. High-intensity pulses induce nonlinear effects that can decrease pulse quality and damage optical components, such as self-phase modulation and self-focusing. CPA takes advantage of chromatic dispersion to temporally stretch an ultrashort pulse and lower its peak power. This is achieved using elements such as grating and prism pulse stretchers which rely on the optical path length difference between the spectral components to introduce chirp and increase the pulse duration. Fibers can also be used to stretch pulses as the refractive index is a function of frequency and so the various spectral components of the pulse will propagate at different speeds.

Once the pulses have been stretched, and the peak power decreased, a laser gain medium can be safely implemented to amplify the pulses. These highly chirped, amplified pulses can then be compressed through dispersion compensation using a grating or prism compressor. The resulting pulse width can be compressed to be similar to that of the input, leading to high-energy and high-peak power pulses.

Chapter 3

Short-Pulse Mid-infrared Generation

Most molecules contain strong, characteristic absorption features in the mid-infrared (MIR) spectral region from 3 - 20 μm, commonly referred to as as the "molecular fingerprint" region. Broadband mid-infrared sources have found use in many applications such as trace-gas detection and spectroscopy, while high-energy MIR pulses see applications in laser wake-field accelerators and surgical lasers to name a few. The generation of mid-infrared light is mainly covered by quantum cascade lasers and nonlinear frequency conversion methods, such as difference frequency generation and optical parametric oscillation. Quantum cascade lasers provide compact and commercially available solutions for MIR generation, while nonlinear frequency conversion methods have yielded more broadband high energy MIR pulses.

3.1 Second-Order Nonlinear Optical Processes

Second-order nonlinear optical techniques [54] such as difference frequency generation (DFG), optical parametric amplification (OPA), and optical parametric oscillation (OPO)

are all the result of the induced second order polarization oscillating at a frequency that is the difference between pump and signal frequencies. Recall that the nonlinear induced polarization can be described as a power series in the electric field strength $\tilde{E}(t)$ as seen in equation (2.1).

These processes can be understood by considering the interaction of two frequency components from an incident optical field in a nonlinear medium, such as a GaSe crystal, for example. We can insert the electric field, represented by

$$\tilde{E}(t) = E_1 e^{-i\omega_1 t} + E_2 e^{-i\omega_2 t} + c.c \tag{3.1}$$

into the second order contribution of the induced polarization. Expanding out $\tilde{P}^{(2)}(t) = \epsilon_0 \chi^{(2)} \tilde{E}^2(t)$ allows us to see the amplitudes of each frequency component of the polarization, given by

$$\begin{aligned} P(2\omega_1) &= \epsilon_0 \chi^{(2)} E_1^2 \quad (i) \\ P(2\omega_2) &= \epsilon_0 \chi^{(2)} E_2^2 \quad (ii) \\ P(\omega_1 + \omega_2) &= 2\epsilon_0 \chi^{(2)} E_1 E_2 \quad (iii) \\ P(\omega_1 - \omega_2) &= 2\epsilon_0 \chi^{(2)} E_1 E_2^* \quad (iv) \\ P(0) &= 2\epsilon_0 \chi^{(2)} E_1 E_1^* + E_2 E_2^* \quad (v) \end{aligned} \tag{3.2}$$

Equations (i) and (ii) represent the amplitudes of the physical process of second-harmonic generation for each of the two distinct frequency components of the incident field. The processes of sum-frequency generation (SFG) and difference frequency generation (DFG) are described by (iii) and (iv) respectively and optical rectification is represented by (v). For each of these processes, the two interacting field components of amplitudes E_1 and E_2 correspond to pump and signal fields of amplitude E_p and E_s.

Specific phase-matching conditions are required for any of these nonlinear optical interactions to occur efficiently, meaning that only one of the nonzero frequency component processes will occur with any significant intensity at a time. The phase matching condition is met by adjusting the input signals polarization and the nonlinear medium's orientation.

3.1.1 Difference Frequency Generation

Difference frequency generation (DFG) is used as a simple, compact solution for mid-infrared sources. This method is based on frequency mixing a pump and signal field, which are spatially and temporally overlapped, in a nonlinear crystal to produce the desired mid-infrared radiation. The generated mid-infrared frequency, sometimes referred to as the idler frequency, is given by the difference of the pump and signal frequencies.

The multi-step process of DFG begins with the higher frequency input field ω_p being absorbed by the atom of a $\chi^{(2)}$ crystal, exciting it to a virtual energy level. An incoming lower frequency ω_s photon then stimulates a two-photon emission process of decay from the highest virtual energy level, down to the ground state with an intermediate virtual energy level in between. This process firsts emits another ω_s photon before emitting a photon of frequency ω_i. This idler output frequency is then given by $\omega_i = \omega_p - \omega_s$. Note that the incoming pump photon is destroyed while another signal photon is generated in this process, effectively amplifying the signal frequency ω_s. This process is therefore also known as optical parametric amplification.

The difference frequency generated power P_i is given by the product [2]

$$P_i = \eta \times P_p P_s \tag{3.3}$$

where P_p and P_s represent the pump power and signal power respectively and η represents a conversion efficiency factor given by

$$\eta \propto \omega_i^2 \left(\frac{d_{eff}^2}{n^3} \right) \frac{L^2}{A} \tag{3.4}$$

The conversion efficiency depends on the crystals effective nonlinear coefficient d_{eff}, average refractive index n, interaction length L and the effective cross section of interaction A. Note that the ω_i^2 term shows that the conversion efficiency drastically drops as the generated mid-infrared wavelength is increased.

3.1.1.1 Optical Parametric Amplification

Optical parametric amplification is effectively an identical process to difference frequency generation, with a strong pump being input into a nonlinear crystal to provide single pass amplification of a signal frequency and generating idler frequency in the process. The objective of OPA is generally to amplify an initially weak signal pulse using strong pump pulses. The distinct feature of the optical parametric amplification regime is that the amplification of the signal pulses scales exponentially relative to the input pump energy [55], whereas under the linear regime of difference frequency generation, the idler and signal grow linearly with increasing pump energy.

3.1.2 Optical Parametric Oscillation

Optical parametric oscillators utilize an optical resonator around a nonlinear crystal, and with the presence of signal and idler fields, stimulated emission of photons at frequencies ω_s and ω_i can occur. Radiation of these desired frequencies can then build to high powers and act as an optical parametric oscillator.

The optical resonator surrounding the nonlinear crystal can be set up with end mirrors which are highly reflective for both the signal and idler frequencies, or the end mirrors can be chosen such that they are only highly reflective of one frequency or the other. The former case is known as a doubly resonant oscillator while the latter is referred to as a singly resonant oscillator. Generally speaking, there are many cavity modes that are supported by the gain profile of an OPO, but in the case of a singly resonant oscillator, it is only the cavity mode which is closest to the peak of the gain curve which will resonantly oscillate as it will take most of the pump power, leaving the other cavity modes to stay below the threshold for oscillation. A doubly resonant oscillator, on the other hand, supports oscillation for both signal and idler frequencies, neither of which are closest to the peak of

the gain curve. This results in oscillators that are less stable under tuning, relative to the singly resonant oscillator.

Optical parametric oscillator systems are often the choices sources for mid-infrared if one is looking for high average power or high peak power in the MIR, but this comes at the cost of requiring an external cavity. OPOs are tunable systems, but they generally don't offer the same tunability within the MIR spectrum that DFG systems do.

3.2 Phase Matching

For the processes of difference frequency generation and optical parametric oscillation, conservation of energy tells us that $\omega_p = \omega_s + \omega_i$. The condition for achieving perfect phase matching for collinear beams, or parallel vectors, is when

$$\Delta k = k_p - k_s - k_i = 0 \tag{3.5}$$

where k corresponds to the magnitude of the wave vectors of the electric fields. This is also referred to as photon momentum conservation. With this condition satisfied, energy can be transferred from the incident waves to the generated wave most efficiently. If equation 3.5 is rewritten in terms of the frequency dependant refractive index, the wave vector mismatch is then given by

$$\frac{n_i\omega_i}{c} = \frac{n_p\omega_p}{c} - \frac{n_s\omega_s}{c} \tag{3.6}$$

since $k = n\omega/c$. This can be simplified to $n_i\omega_i = n_p\omega_p - n_s\omega_s$. Achieving this perfect condition for phase matching is impossible under normal optical conditions since, under normal dispersion, the refractive index increases as a function of frequency.

Phase matching can be achieved by utilizing birefringent crystals since their index of refraction is dependant on the direction of polarization of the optical radiation, rather than on the frequency. Midwinter and Warner [56] described two types of phase matching:

type-I phase matching where the two fields have the same polarization (i.e. both ordinary or extraordinary rays) and type-II phase matching where the fields are orthogonally polarized (i.e. one is an ordinary ray while the other is extraordinary). Angle tuning of the crystal, with respect to the direction of propagation of the incident light, allows one to control the refractive indices required for the desired frequencies. The downside to this method is spatial walk-off, which occurs when the Poynting vector and the wave vector are propagating at an angle to each other for extraordinary rays. This can effectively limit the spatial overlap of the two incident waves.

3.2.1 Quasi Phase Matching

An alternative method for achieving photon momentum conservation is by using quasi phase matched crystals [2]. These crystals contain periodic reversals of the sign of the optical nonlinearity which are created by periodically inverting the crystalline orientation. This grating inside the crystal can compensate for the wave-vector mismatch by correcting the relative phase at regular intervals, determined by the grating period Λ. In order to achieve quasi-phase matching, the periodicity in the crystal should be such that equation 3.5 becomes

$$\frac{2\pi}{\Lambda} = k_p - k_s - k_i \tag{3.7}$$

and, therefore, compensates for the wave vector mismatch.

3.3 Mid-infrared generation from optical parametric oscillator systems

OPO-based mid-infrared sources are generally used for wavelengths below 5 μm due to the combination of a limited transparency range for commercially available nonlinear crystals

and the limited spectral range of the optical resonator [57]. Even with nonlinear crystals that can support wide spectra, tunability of OPOs is limited by the bandwidth of the mirror coatings. However, long-wavelength MIR was succesfully demonstrated in 2018 by Maidment et al. [58]. They utilized an orientation-patterned gallium phosphide (OPGaP) for their OPO system due to its long wavelength transparency. This allowed them to yield an idler output which was tunable from 5.5 - 11.8 μm at room temperature using different gratings. They recorded a maximum power of 105 mW at 5.5 μm. They were able to yield MIR past 13 μm by incorporating temperature tuning.

Beutler et al. have demonstrated wide tuning ranges within the MIR spectral range with mW level powers using difference frequency generation of dual-wavelength OPO systems. In 2015 [59], they generated MIR which was tunable from 5 – 18 μm using an Yb-fiber laser pumped OPO system. At a wavelength of 6μm, they recorded an average power of 140 mW which, at a repetition rate of 80 MHz, corresponded to a pulse energy of 1.75 nJ. Steinle et al. [60] used a combination of OPO and OPA systems to obtain their signal and idler frequencies. They then generated highly stable 350 fs MIR pulses by difference frequency mixing their outputs to obtain gap-free tunability from 1.33 – 2.0 μm with up to 2.8 W of power and 2.13 – 20 μm with tens of milliwatts of power.

3.4 Mid-infrared generation from ultrafast Ti:sapphire laser systems using DFG

Difference frequency generation based MIR sources were commonly created using two-colour ultrafast Ti:sapphire laser systems in earlier works. In 1995, de Barros et al. [61] demonstrated femtosecond MIR pulses which were tunable from 7.5 – 12.5 μm with an average power of 5 μW at a wavelength of 10 μm. This was achieved by difference frequency generation of the output from a two-colour Ti:sapphire laser in a 1 mm thick $AgGaS_2$ crystal. Today, GaSe remains the more popular choice for generating mid-infared through

difference frequency generation, the advantages of which were demonstrated by Ehret et al. in 1998 [62]. They used a Ti:sapphire laser to pump a dual-wavelength OPO, the output of which they difference frequency mixed in a 1 mm thick GaSe crystal. Their system yielded tunability from 5.2 – 18 μ with a maximum average power of 2 mW at 8.5 μm. The GaSe crystal proves to be more efficient throughout the entire spectral range compared to the $AgGaS_2$ due to its higher nonlinearity and increased transparency above 10 μm. Donna Strickland's group incorporated a two-colour Ti:sapphire laser to create a DFG-based mid-infrared source emitting high energy pulses around 10 μm [63]. Both output pulses from the two-colour laser, set at 800 and 870 nm, were simultaneously amplified in a regenerative amplifier before being mixed in a 1-mm $AgGaS_2$ crystal. Their system produced MIR pulses in the 9 – 11 μm range with up to 1.6 μJ of energy.

3.5 Mid-infrared generation from ultrafast fiber laser systems using DFG

The use of ultrafast fiber lasers in difference frequency generation based mid-infared sources has become more common due to their high average powers, excellent heat dissipation, and the overall compactness of all-fiber systems. A high power Yb-fiber laser system, emitting 480 nJ femtosecond pulses, was used by Zhou et al. [64] in 2018. By utilizing a polarizing beam splitter, they split the output of the Yb:fiber laser source. One arm was fiber-coupled into a large-mode-area fiber (LMA) fiber where spectral broadening through self-phase modulation occurred. This broadened beam acted as their signal, while the other arm served as their pump in the process of difference frequency generation. They achieved tunability from 7 – 18 μm with a maximum average power of 5.4 mW at 9.5 μm.

Sotor et al. were the first to demonstrate a fully all-fiber DFG-based MIR source [65], with the entire pumping laser being built from single-mode, polarization-maintaining fibers. Each branch from the lasers seed output was separately amplified before being recombined

into a single-mode fiber using a wavelength division multiplexer. They incorporated a fiber-coupled variable delay line to account for the temporal overlap, demonstrating tunability from 6 – 8.8 μm with a maximum average power of 7.4 mW at 7.5 μm. Donna Strickland's ultrafast laser team also made the switch to a partially fiberized system [24, 66] after mostly using bulk-optic elements in the past. A chirped fiber Bragg grating was used to filter out a 60 nm notch from a spectral continuum, with colours centered at 1024 and 1088 nm. The two colours were then amplified by a fiber-coupled CPA system before being difference frequency mixed to generate long-wavelength MIR. They demonstrated 2.5 mW of power at an 18 μm wavelength.

3.6 Mid-infrared generation using optical parametric amplification systems

Optical parametric amplification systems are commonly used as MIR sources, usually with the primary goal of higher energy pulses over achieving broadband tunability. Liang et al. [67] generated 33 μJ energy pulses with 1.9 GW of peak power, covering the spectral range of 2.5 - 9 μm using their OPA system. Seidel et al [68] utilized a PPLN crystal in their OPA system, achieving 5.1 Watts of average power at 4.1 μm. They also generated 1.3 W of power at 8.5 μm using an LGS crystal. Optical parametric chirped pulse amplification (OPCPA) is a technique which combines CPA in an OPA system in order to generate higher energy mid-infrared pulses. This technique involves stretching the pulses before they enter the crystal used for OPA before being compressed through dispersion compensation, yielding high energy MIR pulses. An OPCPA system was used by Elu et al. [69] to achieve 0.75 mJ pulses at 7 μm, corresponding to the highest energy pulses demonstrated at that wavelength to date.

3.7 Mid-infrared generation using intra-pulse difference frequency generation systems

Intra-pulse difference frequency generation (IDFG) has made significant progress as a method of achieving MIR pulses in recent years. This technique entails mixing the spectral components from within the same broadband near-infrared femtosecond pulse in a nonlinear crystal to generate MIR. This technique has produced MIR sources that cover a wide range of the molecular fingerprint while maintaining high powers and excellent phase stability. IDFG also has the advantage of demanding a lower footprint compared to other nonlinear conversion techniques due to the necessity of only one pump laser and a nonlinear crystal.

IDFG has been succesfully implemented to yield pulses which have covered nearly the entire molecular fingerprint region from 4-20 μm [70],[71]. Zhang et al. successfully produced a continuous broadband MIR spectrum which covered the 4.5 - 20 μm region with over 24 mW of average power [71]. An all-fiber single-cycle 100 MHz frequency comb was recently demonstrated by Xing et al. [72] which they utilized for intra-pulse difference frequency generation, producing MIR pulses spanning 6 - 25 μm with 270 μW of power. Most recently, Kassab et al. [73] demonstrated IDFG driven in two nonlinear crystals, LIO and LGS, set in a collinear fashion. They achieved a spectral span covering 3.4 - 15 μm while maintaining 130 mW of MIR power.

High energy microjoule MIR pulses have been achieved through IDFG. Liu et al. [74] achieved a record high IDFG conversion efficiency of 5.3% by utilizing a longer driving wavelength of 3 μm from an OPCPA system which produced 10 kHz, 95 μJ, 35 fs pulses, effectively lowering the quantum defect of the system compared to driving at 1 μm. Upon sending these pulses through a GaSe crystal, MIR pulses spanning 6 - 13.2 μm were produced with 5 μJ of energy. Butler et al. achieved a broadband high-power MIR source using a 2 μm fiber laser to pump a GaSe crystal. They reached the long wavelengths of

the molecular fingerprint region with the pulses covering 6 - 18 μm while maintaining 498 mW of average power and 43 fs pulse duration. Bournet et al. [75] recently demonstrated a technique for optimizing the conversion efficiency of IDFG which resulted in an improvement by a factor of 2.5. They utilized a multi-order wave plate before their GaSe crystal, allowing them to selectively rotate the pump and signal photons to achieve a more optimal phase matching configuration. This led to an increase in average power from 8.1 mW to 20 mW, demonstrating a relatively simple method for increasing the power of IDFG MIR sources.

3.8 Quantum Cascade Lasers

Quantum cascade lasers (QCL) utilize electrons as charge carriers to generate photons as they transition between the intersubbands of multiple-quantum-well structures. Using various semiconductor materials, the active region is engineered with nanoscale alternating wells and barriers to artificially create these energy levels [76]. With an appropriately applied voltage, electrons travel perpendicularly through the layers of the active region. Once a photon is emitted, the electron remains in the conduction band as it is injected into the neighboring active region, producing a cascading effect whereby one electron emits a photon at each adjacent stage of injector and active regions. Lasing is achieved by the 3-level structure of the active regions where the difference in energy between level 3 and 2 is determined by the thickness of the walls, and levels 2 and 1 are separated by about an optical phonon energy. Since the relaxation time between energy levels 3 and 2 is much longer than the lifetime of state 2, a population inversion can be realized.

Faist et al. [77] invented the quantum cascade laser in 1994 where they demonstrated a peak power of 8 mW at 4.2 μm. They recognized the technological significance of this type of laser as they noted that the output wavelength was solely dependant on the design of the quantum wells. Hofstetter et al. [78] showed a major improvement in performance

by using a 4-level quantum well instead of the standard 3-level system. The lower 3 energy levels of their design were separated by one phonon energy, yielding what they referred to as double phonon resonance. This design maintained the injection efficiency of the 3-level design while shortening the lifetime of the lower lasing state and thereby creating a larger population inversion. They achieved 1.15 W of peak power at a wavelength of 5.3 μm. Quantum cascade lasers became more efficient over time with significant increases in power. Razhegi et al. [79] achieved 4.9 μm pulses with 34 W of peak power. An average power of 3W in CW operation of a mid-infrared QCL has also been demonstrated [80].

With trace-gas analysis and spectroscopy being some of the most desired applications of mid-infrared sources, providing broad tunability within the mid-infrared spectral range is required. By implementing an external cavity and a bound-to-continuum design of the active region, Maulini et al. [81] demonstrated tuning from 4.94 - 5.4 μm from their QCL. The external cavity allowed the selection of any wavelength within the QCL's gain bandwidth while the bound-to-continuum design provides the broad spectrum by having the lower state of the laser transition consist of many sublevels. Improving upon this design, Wittmann et al. [82] achieved tunability from 7.66 - 9.87 μm with a peak power of 800 mW. Hugi et al. [83] introduced multiple substack active region designs where each substack emits at different wavelengths, furthering the broadband tunability of QCLs. With this design, they achieved tuning from 7.6 - 11.4 μm with a peak power of 1 W at 8.47 μm. A 6 stage substack design was implemented more recently by Bandyopadhyay et al. [84] which allowed them to emit from 5.9 - 10.9 μm with peak powers of 300 mW.

Chapter 4

Experimental Setup and Results

This chapter begins by discussing the setup and performance of the all-normal dispersion fiber laser as well as the gain-managed nonlinear amplifier that are implemented for our two-colour experiments. The ANDi output serves as the seed for the GMNA which then provides an amplified and broadband output from which we can select our two-colours. The various methods of two-colour selection and amplification are then discussed. First, attempts at amplification in the 10-micron core Yb-doped fiber are discussed, followed by the results of amplifying in a 30-micron core fiber in which we saw more success.

4.1 All-Normal Dispersion Fiber Laser

A schematic of the all-normal dispersion fiber laser used in our experimental setup is shown in figure 4.1. The four main elements of an ANDi laser can be visualized with the first section being the long segment of single mode fiber. This section contains a fiber collimator which leads to a segment of passive HI-1060 fiber. The length of this passive fiber can be adjusted based on the desired repetition rate of the ANDi by altering the total cavity

length. In our setup, approximately 15 m of passive fiber is used, yielding a 9.68 MHz repetition rate which will be discussed shortly. A multi-mode pump fiber is used to deliver pump power efficiently to the system and is joined to the passive fiber through a combiner. The combiner takes the passive fiber as input and sends the light to the core of its output fiber. The pump light is delivered to the cladding of the combiner's output fiber. This first section of the ANDi ends with the output of the fiber combiner.

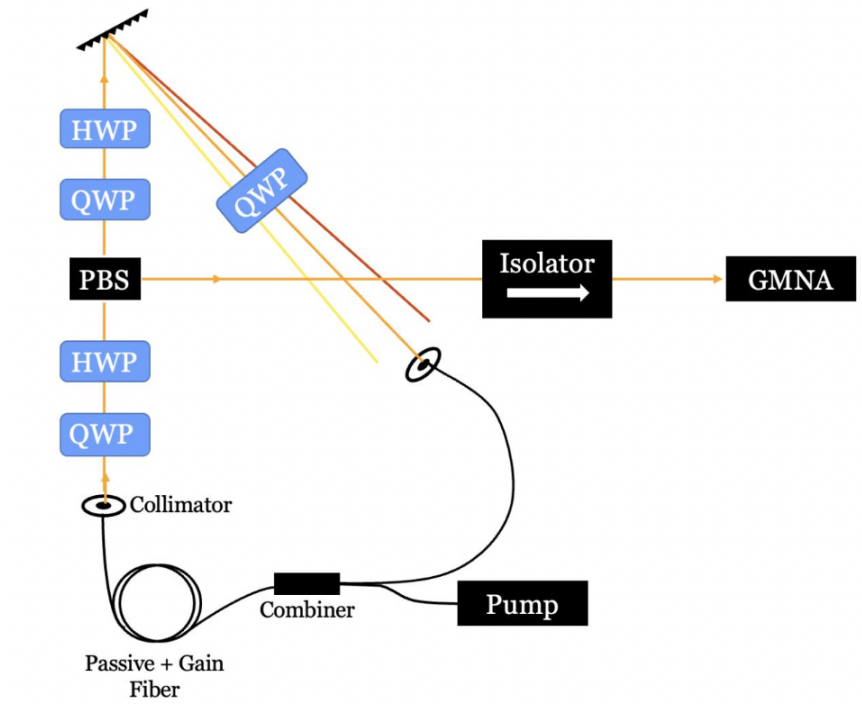

Figure 4.1: Schematic of ANDi fiber laser used in our experimental setup. Quarter Wave Plate (QWP), Half Wave Plate (HWP), Polarizing Beam Splitter (PBS), Gain-Managed Nonlinear Amplifier (GMNA)

The next section of our ANDi simply consists of the gain fiber. For our setup we are utilizing a 0.5 m segment of double-cladded Yb-doped fiber with a core diameter of 6 μm and an outer cladding diameter of 125 μm. As discussed in section 2.2, Yb-doped fibers contain strong absorption at 976 nm, allowing them to be efficiently pumped at this

wavelength for generating pulses at wavelengths around 1030 nm.

The gain fiber precedes a short segment of passive single-mode fiber which is spliced to the gain fiber and surrounded by index-matching gel. This gel serves to remove any residual pump light that is present at the end of the gain fiber, leaving only the amplified seed to be transmitted through the single-mode fiber and into the final free space region of the ANDi. The gel contains the same refractive index as that of the outer cladding of the fiber, allowing the pump light to be transmitted and then absorbed by the splice covering. The transmitted seed then passes through a fiber collimator and enters the final segment of the ANDi; the nonlinear polarization evolution (NPE) region.

The NPE region in our experimental setup consists of two half-wave plates (HWP), two quarter-wave plates (QWP), a polarizing beam splitter (PBS) and a dispersion grating. Referring to figure 4.1, one can see that the QWP and HWP follow the fiber collimator of the second single-mode fiber region and precede the PBS. As discussed in section 2.6.2, these wave-plates serve to control the polarization of the propagating light such that the polarization with the highest optical intensity experiences the lowest loss and gets transmitted as the reflected beam of the PBS. This serves as the ejection port of the NPE region and continues to a free space isolator which marks the overall output of the ANDi. This combination of wave-plates and a PBS act as a saturable absorber and allow for passive-modelocking to be achieved.

The light that is transmitted through the PBS passes through a second half-wave plate which is not required for mode-locking but rather serves to match the required polarization of the grating. This dispersion grating is then used for spectral filtering by placing the grating further or closer to the input fiber collimator of the first single-mode fiber segment of the ANDi. The spatial chirp that the dispersion grating provides allows us to select the bandwidth of light entering the fiber, and improve the stability of the mode-locking state. The second quarter-wave plate is placed after the grating, ensuring circular polarization enters the single-mode fiber.

4.1.1 Mode-locking state

A stable mode-locking state can be identified by its pulse train in the time domain and its output spectrum characteristics. A photodiode connected to an oscilloscope is used to monitor the pulse train, as shown in figure 4.2a. A mode-locked state is identified by stable pulses of relatively equal amplitudes with no multi-pulsing occurring and a displayed repetition rate that is consistent with the cavity length. The ANDi used in this experimental setup has a repetition rate of 9.67 MHz, with a pulse duration of 6 ps and an output average power of 50 mW.

A spectrometer is used to observe the ANDi's output spectrum. As discussed in section 2.6.3, as spectral filtering is appropriately applied in the ANDi and a stable modelocking state is reached, the spectrum displays a characteristic double-peak feature which is indicative of the self-phase modulation that occurs. The ANDi's output spectrum is centered at 1030 nm with a 10 nm bandwidth, consistent with the expected bandwidth for a stable state mentioned in section 2.6.3.

4.2 Gain-Managed Nonlinear Amplifier

The output of the all-normal dispersion laser is seeded into the gain-managed nonlinear amplifier (GMNA), with the goal of creating a powerful, broad spectrum from which to select two colours from. The schematic of our GMNA setup is seen in figure 4.3. As discussed in section 2.5, a GMNA should be seeded with a narrowband short pulse, usually with a pulse duration around 1 ps. This is so the pulses enter the fiber with sufficient peak power to induce the desired self-phase modulation for broadening. Since the ANDi outputs 6 ps pulses, a grating compressor is incorporated as the first element after the ANDi. The pulses are compressed before passing through a band-pass filter (BPF) which is used to reduce the bandwidth down to approximately 4 nm. The angle of the BPF can be adjusted

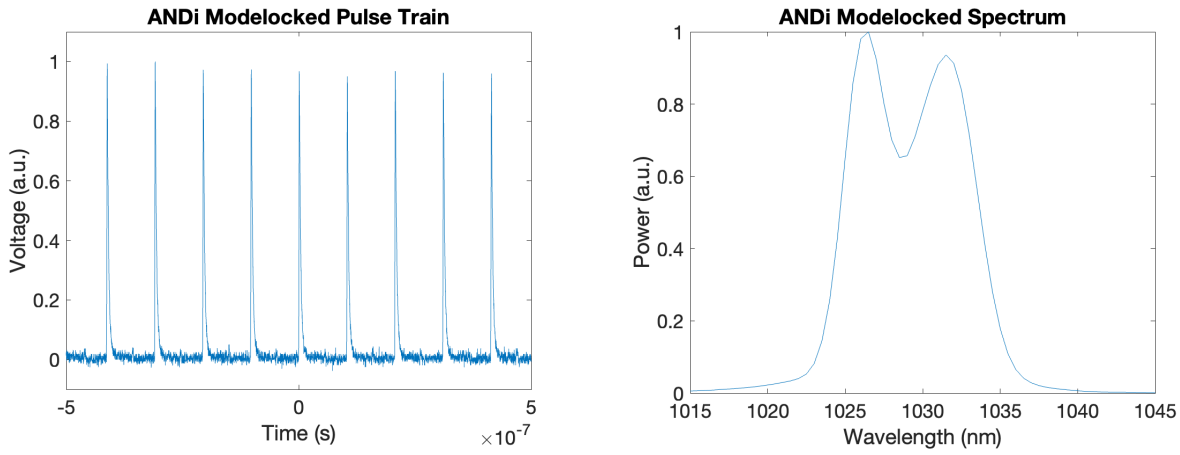

(a) (b)

Figure 4.2: Modelocked state of the all-normal dispersion fiber laser showing the (a) modelocked pulse train with a repetition rate of 9.67 MHz and (b) the modelocked output spectrum with characteristic double peak

to achieve the desired center wavelength for optimal spectral broadening of the GMNA. The pulses then pass through a half-wave plate which is used to align the polarization with the appropriate axis of the polarization-maintaining gain fiber. The pulses, now with the correct polarization, are joined by a 976 nm pump diode in a combiner which outputs both into a PM-Yb-doped fiber. The optimal length of gain fiber is determined through simulations based on the input seed. With the correct input seed characteristics, this is where the gain-managed nonlinear amplification occurs.

Optimal spectral broadening was achieved by observing the output spectra while adjusting both the BPF and the HWP. By slowly increasing the pump power, and making small readjustments to these components, a broad spectrum could be achieved without surpassing the upper limit of power. As discussed earlier in section 2.5, the power is limited by noise-induced Raman scattering which is characterised by a red sideband that begins to develop. Figure 4.4 shows the linear and log plots of the GMNA spectra achieved in our experiment. The spectral broadening quickly increases as the pump power is increased

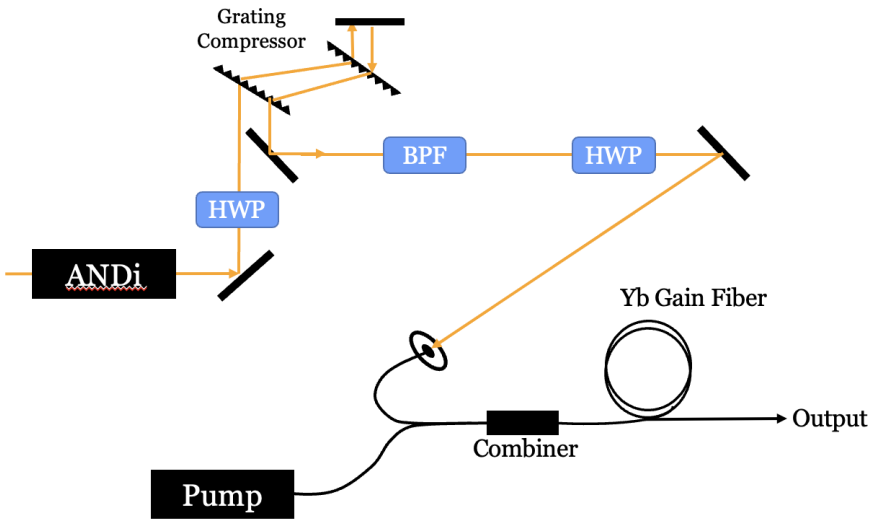

Figure 4.3: Schematic of gain-managed nonlinear amplifier (GMNA) used in experimental setup with a grating compressor being used to decrease the pulse duration in order to increase the peak power for desired nonlinear effects.

with a noticeable decrease in broadening occurring from 4 to 4.5 W of pump power. This is where the upper limit of power is achieved as the Raman-induced sideband is clearly seen to develop at 4.5 W. At 4.5 W, a bandwidth of 120 nm is achieved with an output power of 2.1 W. This GMNA output was used for most of the two-colour experiments that will be discussed in the following sections.

The required grating-to-grating distance in the compressor was calculated and implemented with the goal of decreasing the pulse duration to be near 1 ps. However, due to a miscalculation, the pulse was over-compressed and likely negatively chirped going into the GMNA fiber. Furthermore, the isolator that was implemented after the ANDi was damaged and was emitting elliptical polarization instead of linear. This meant that we were unable to utilize the polarization maintaining properties of the Yb-fiber and had elliptical polarization coming out of the GMNA. Since a free-space isolator was implemented after the GMNA to prevent damage from back-reflections, the usable power from the GMNA was cut by approximately half since the isolator is made up of two polarizing beam split-

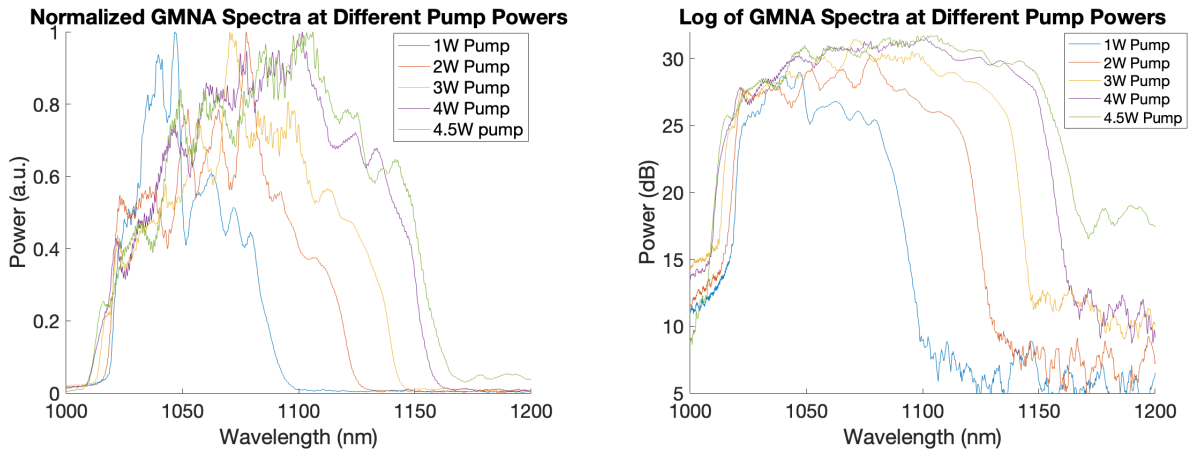

(a) (b)

Figure 4.4: Spectral broadening of the GMNA based on different pump powers demonstrated in a (a) linear plot and (b) log plot. The upper limit of pump power is demonstrated by the development of the red sideband at 4.5 W of pump power, seen clearly in the log plot.

ters. This meant that of the 2.1 W coming out of the GMNA, only 860 mW actually made it through the isolator and into our two-colour experiment.

Upon changing the isolator that follows the ANDi output, and correctly implementing the grating compressor, a new GMNA output could be realized which maintained its linear polarization. The pulse was compressed from 6 ps down to 1.7 ps before being sent to the GMNA. As seen in figure 4.5, a similar bandwidth of 120 nm is achieved but at a lower pump power of 2.5 W. This is where the same red sideband begins to appear, indicating that we have reached the power limit. At a pump power of 2.5 W, the GMNA outputs 1.1 W of power with a 2.8 ps pulse duration. Since linear polarization is maintained, the power that reaches the two-colour experiments is now only limited by the efficiency of the free-space isolator, meaning that at only 2.5 W of pump power, over 900 mW of usable seed power is available.

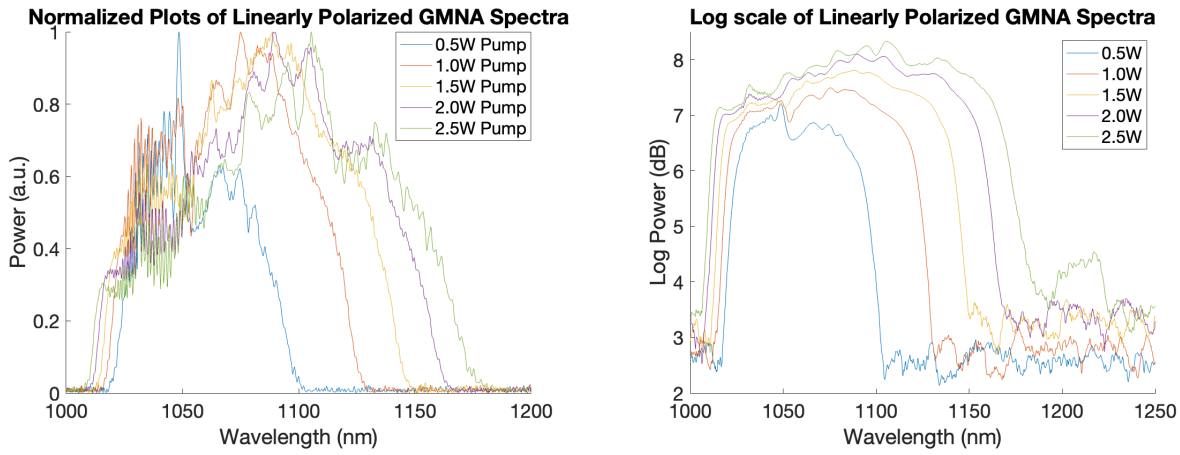

(a) (b)

Figure 4.5: Spectral broadening of the linear polarization maintaining GMNA based on different pump powers demonstrated in a (a) linear plot and (b) log plot. The upper limit of pump power is demonstrated by the development of the red sideband at 2.5 W of pump power, seen clearly in the log plot.

4.3 Two-Colour Selection and Nonlinear Amplification

Upon obtaining a broad spectrum of over 120 nm of bandwidth from our gain-managed nonlinear amplifier, we can select two colours which can then be amplified and eventually used for MIR generation through difference-frequency generation. One can do this by creating a two-colour chirped pulse amplifier, but these systems inevitably suffer from gain narrowing, limiting the pulse duration and the tunability of the generated MIR. Our goal was to take advantage of the nonlinear effects that can occur in the gain fiber to combat the gain narrowing while simultaneously amplifying each of the two colours. By cutting out the center of the spectrum, each of the two colours could then get gain without the center wavelengths overpowering the outer wavelengths which are used for DFG. This section will outline the various experimental setups and results achieved in our quest to develop a

two-colour nonlinear amplifier for MIR generation through DFG.

4.3.1 Two-Colour Amplification in 10/125 μm Yb Fiber

4.3.1.1 CFBG Two-Colour Selector and Amplification

The first experimental setup for the two-colour selector utilized a custom chirped fiber bragg grating (CFBG). This was implemented with the goal in mind of eventually creating an all fiber system where the output of our GMNA could be spliced to the CFBG which would then connect to the two-colour fiber amplifier through a combiner. Initially, the CFBG was not removing the center wavelengths as intended until a 100 m passive fiber was included before it. This indicated that the pulse duration coming out of the GMNA was too short, and the peak power too high, for the CFBG to be effective. The schematic of the CFBG selector and amplifier can be seen in figure 4.6a. The two-colour input was seeded into a 17-m Yb-doped fiber with a 10-μm core and 125-μm outer cladding diameter before being counter-pumped by a 975-nm laser diode. The amplified two-colour output can be seen in figure 4.6b.

The CFBG cut out a 40-nm notch from the broad GMNA spectrum, yielding two colours centered at 1070-nm and 1110-nm. These two-colours were then amplified by counter-pumping up to 8.4 W. It is clear from figure 4.6b that there are little to no nonlinear effects at work during amplification, leaving the two-colour spectrum to amplify as it would under a CPA-regime. This is expected as the 100-m passive fiber was used to increase the pulse duration and, therefore, decrease the peak power. We observe the blue colour taking most of the gain as it is much closer to the emission peak of Ytterbium at 1030-nm, as discussed in section 2.2. We, understandably, do not observe any broadening in the two-colour spectrum.

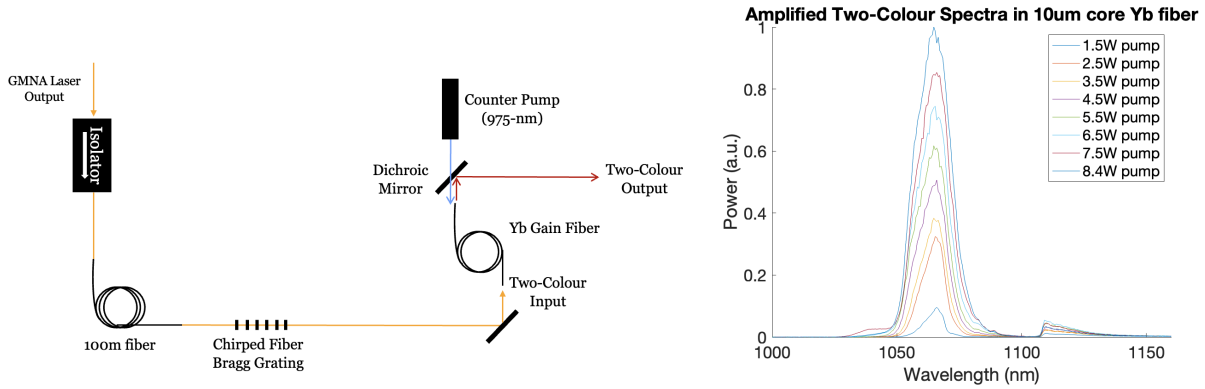

(a) (b)

Figure 4.6: Two-colour selection and amplification using a chirped fiber bragg grating (CFBG) as the two-colour selector. Schematic (a) of selector and amplifier is shown along with the resulting amplified spectra (b) pumped up to 8.4 W

4.3.1.2 Notch Filter Two-Colour Selector and Amplification

We then implemented a notch filter instead of the CFBG as a two-colour selector. This allowed us to remove the 100-m passive fiber and retain the 6-ps pulse duration that is coming out of the GMNA. The schematic of the experimental setup is shown in figure 4.7. The notch filter selects two-colours centered at 1030-nm and 1110-nm, the spectrum of which can be seen in figure 4.8a. This spectrum is then seeded into the same 10/125 Yb-fiber and counter-pumped with up to 8.5-W of power. The amplified two-colour spectra can be seen in figure 4.8b. The notch is quickly filled in as the pump power is increased, with the final 8.5-W amplified spectrum having completely lost its two-colour characteristics. This indicates that there is likely too much self-phase modulation occurring as the pulse intensity is too high for the 10-micron diameter core.

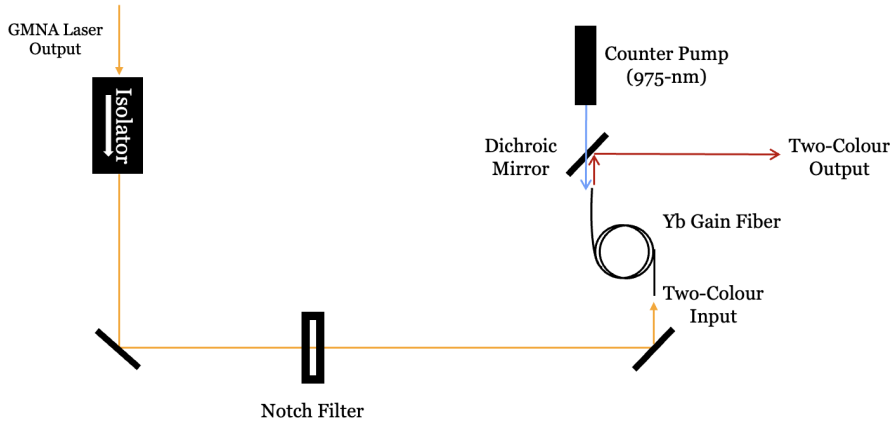

Figure 4.7: Schematic of two-colour selector and amplifier using notch filter and a 10/125 μm Yb fiber

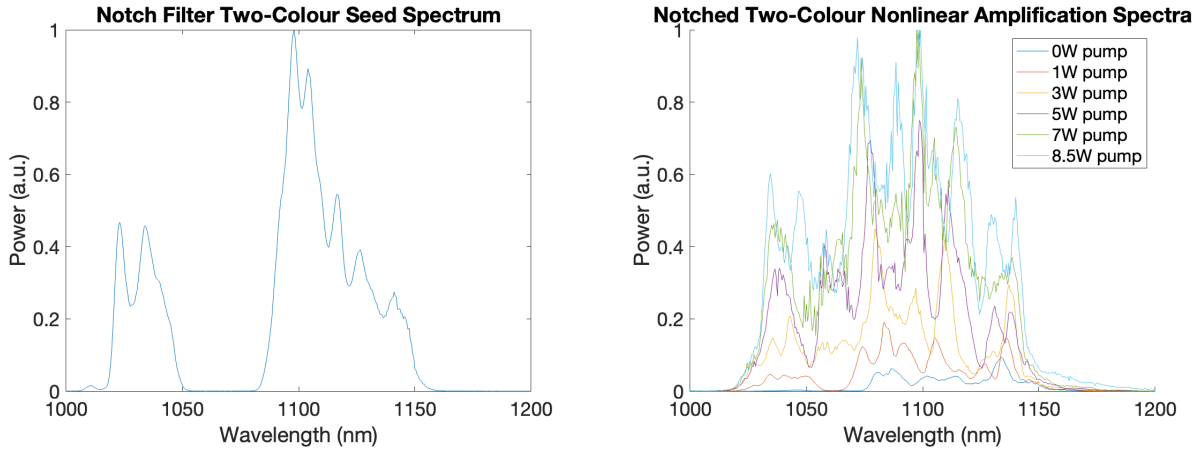

(a) (b)

Figure 4.8: Two-colour selection and amplification using a notch filter as the two-colour selector. Two-colour seed spectrum (a) is shown along with the resulting amplified spectra (b) pumped up to 8.5 W

4.3.1.3 2f System Pulse Shaper Two-Colour Selector and Amplification

Our next experimental setup replaced the notch with a 2f system which consisted of a dispersion grating, lens and a mirror, as seen in figure 4.9. An adjustable beam blocker was set between the lens and the mirror so that the gap between the two-colours could be quickly and easily adjusted. This was done with the idea in mind that we could amplify the incoming two-colour pulses and subesequently adjust the two-colour input to see how it would affect the gain competition occurring between the two colours and the overall two-colour output.

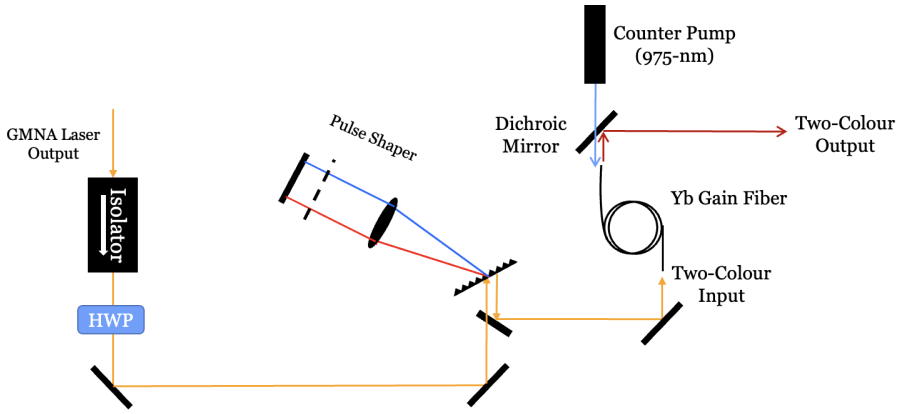

Figure 4.9: Schematic of two-colour selector and amplifier using a 2f system and a beam blocker for pulse shaping. The 2f system consisted of a dispersion grating, a lens, and a mirror, with an adjustable beam blocker set between the lens and mirror.

Another advantage of implementing this setup is that we could separately amplify the red or blue side of our spectrum and observe how they individually evolve under amplification. We set a beam blocker to cut the wavelengths above 1080 nm, and amplified this input seed with up to 8 W of counter-pump. The blue input can be seen in figure 4.10a with the amplified spectra shown figure 4.10b. The blue colour quickly showed broadening towards the red, with wavelengths up to 1100 being quickly generated and amplified. This

is consistent with the results seen in a regular gain-managed nonlinear amplifier, where the blue wavelengths quickly broaden towards the red side through self-phase modulation and then further amplify. As the pump power was increased, gain narrowing was also observed around 1080 nm. The colours below 1050 nm were absorbed, likely due to the 17-m length of the Yb-fiber. Since this is a relatively long gain fiber, the blue wavelengths could be absorbed and acting to pump the red wavelengths by the end of the fiber.

The same experiment was performed where the wavelengths below 1080 nm were blocked to leave only the red side as an input. The input seed can be seen in figure 4.10c which was then amplified with up to 8 W of pump power, as seen in figure 4.10d. No further broadening was seen into the red wavelengths, with little amplification of those wavelengths as well. This is unsurprising as the gain above 1100 nm is relatively insignificant in Yb-amplifiers compared to the shorter wavelengths. We do observe some shifting of the wavelengths below 1080-nm which look like a shift towards the gain peak of Ytterbium.

This 2f experimental setup was implemented with the notch in various positions and widths, but it was observed to be consistently difficult to pump the two-colour input past 3-4 Watts, irregardless of notch characteristics. As the pump power was increased, the two-colour spectrum would quickly fill in the gap, and then become spikey. The spikes would generally be strong enough to warrant having to cut new ends on the fiber to avoid damage-induced losses or obstructions to our results. This further indicated that the incoming pulse intensity was too high for the core diameter of the 10/125 Yb fiber being used. In order to reduce optical intensities inside the fiber, a larger fiber would have to used.

4.3.1.4 Co-pumped Two-Colour Amplification

Switching from counter-pumping to a co-pumping regime yielded similar results. Once again, we observed the gap between the colours get quickly filled in, leaving no benefit to

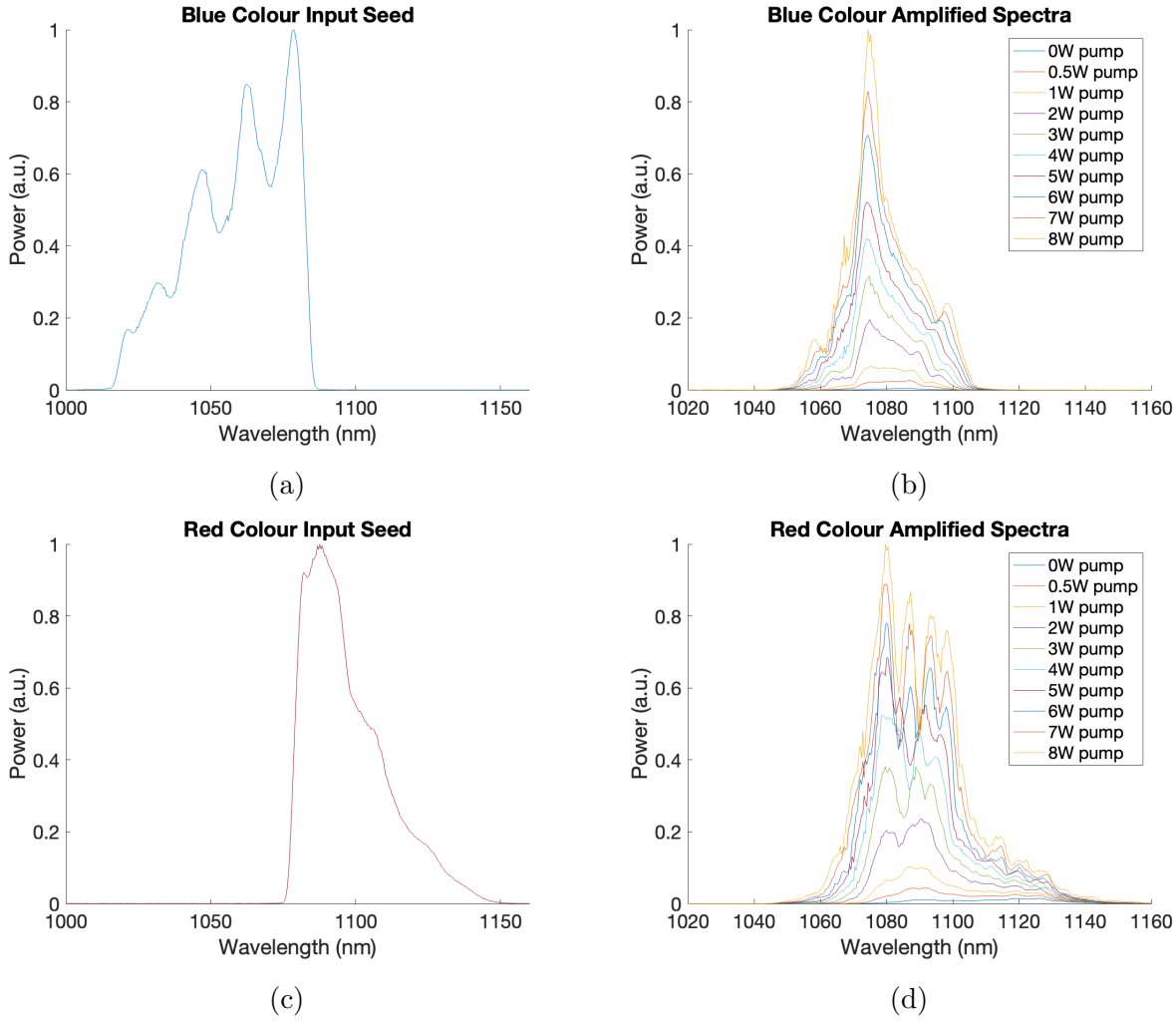

Figure 4.10: Separate amplification of (a) blue input colour and (c) red input colour after making a sharp cutoff at 1080 nm for each respective colour using a beam blocker in a 2f system. Figures (b) and (d) show amplification of each colour with up to 8 W counter pump.

the removal of the central wavelengths before amplification. The fiber was cut down to 3-m, meaning that we should expect to retain more of the blue colour compared to the 17-m fiber where the blue began to get absorbed and act as a pump for the red wavelengths. We were able to pump the selected two-colours with up to 9 W of power, the amplified spectra

of which can be seen in figure 4.11a. This figure shows the amplification of colours all the way up to 1300 nm when pumped at 9W, well past the seeded wavelengths. This can be better understood by looking at the log of these spectra in figure 4.11b. When pumping up to 2 W, there is no notable change in the red side of the two-colour spectrum around 1160 nm. Once we surpass 2 W of pump power, we notice the Raman-induced shoulder beginning to develop on the red side of the spectrum. It quickly builds and continues to grow as the pump is increased to 9 W. As mentioned earlier, this Raman shoulder is induced by shot noise and is incoherent, according to Sidorenko et al.[8]. This was further confirmation that our seed pulse intensity was too high for our 10-μm core diameter as the nonlinear effects were too strong within the fiber.

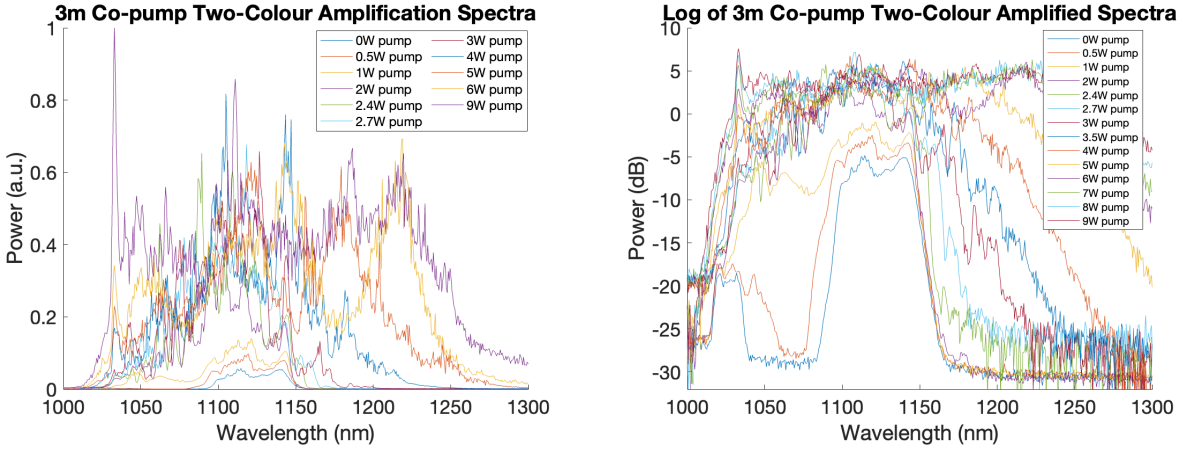

(a) (b)

Figure 4.11: Co-pumping 3 m Yb fiber after selecting two-colour spectrum. Figures show the amplified spectra with up to 9 W of co-pumping (a) and the log of these spectra (b) where the growth of the Raman sideband is evident.

4.3.2 Two-Colour Amplification in 30/250 μm Yb Fiber

In order to decrease the optical intensities inside of our gain fiber, we implemented a 20-m long large-mode-area fiber which still retained single-mode guidance. The fiber, from the

company nLight, is polarization-maintaining and has a 30-μm core diameter with a 250-μm outer cladding diameter. This implies a higher damage threshold and weaker nonlinear effects.

4.3.2.1 20-m Yb Fiber Two-Colour Amplification

The first experimental setup implemented with the 30-micron fiber involved counter-pumping the 20-m fiber after selecting the two colours from our GMNA output using a notch filter. The notch filter removed a 40-nm gap from the spectrum leaving a two-colour seed with peaks at 1040 nm and 1100 nm, corresponding to a 60-nm peak-to-peak separation. This seed was then coupled into the Yb fiber in free space using a fiber mount and amplified with up to 20W of counter-pump, the amplified spectra of which can be seen in figure 4.12.

At 20 Watts of pump power, the seed spectrum was amplified to 2.9 W. Although the amplified spectra look promising, with the blue colour broadening towards the longer wavelengths and the red colour retaining its bandwidth under amplification instead of gain narrowing, the blue colour was later determined to be comprised of amplified spontaneous emission (ASE) and not amplified seed wavelengths. By adjusting the notch filter while under amplification, we observed that altering the two-colour input affected the amplified red colour characteristics while the blue colour retained its characteristics, regardless of input. This implied that it was only ASE that we were seeing in the blue wavelengths of our amplified output.

Since the gain fiber is rather long at 20 m, it is possible that the pump power was not making it all the way to the end of the fiber and was being fully absorbed at some point in the fiber. Since we are counter-pumping, this would imply that the beginning of the fiber would only serve to absorb the two-colour seed and would absorb the blue colour much faster, as understood by the absorption profile of Ytterbium. The output of the fiber would

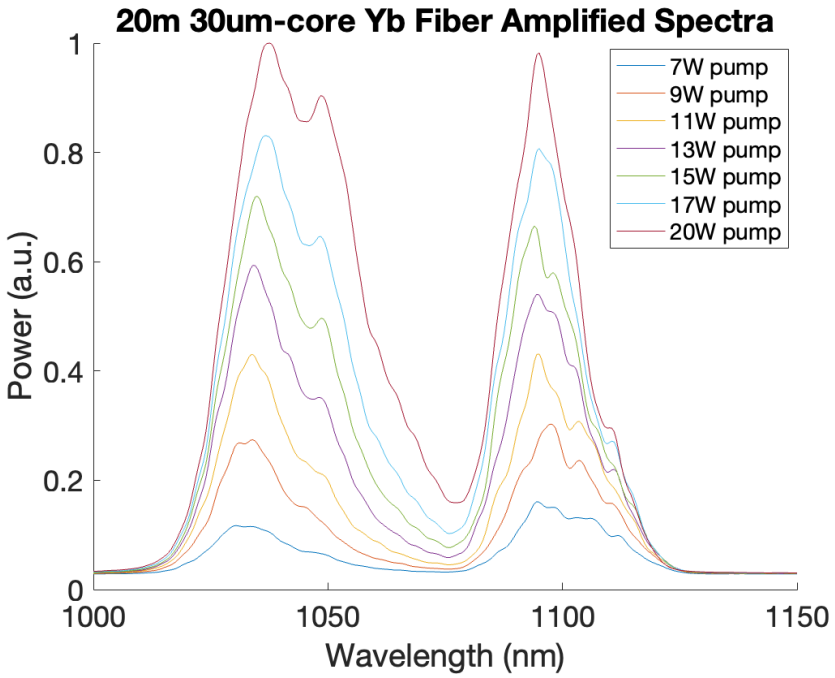

Figure 4.12: Amplification of two colour spectra in 20-m of 30-μm core Yb fiber with input colours set at 1040 nm and 1100 nm using notch filter.

then only have the remaining red colour amplified, along with the amplified spontaneous emission which out-competed the blue colour for gain in the early stages of the fiber.

4.3.2.2 14-m Yb Fiber Two-Colour Amplification using Fiber Combiner

The fiber was cut down to 14 m in an attempt to retain and amplify the blue wavelengths of our input seed. Furthermore, a fiber combiner was implemented such that the pump fiber and the Yb-doped gain fiber could be spliced onto the combiner, resulting in stronger pump coupling since we were no longer relying on free-space fiber coupling for the pump. A notch filter was again used to cut out a 40-nm gap from 1050 - 1090 nm before being counter-pumped with up to 20 W of power. The amplified spectra can be seen in figure 4.13a.

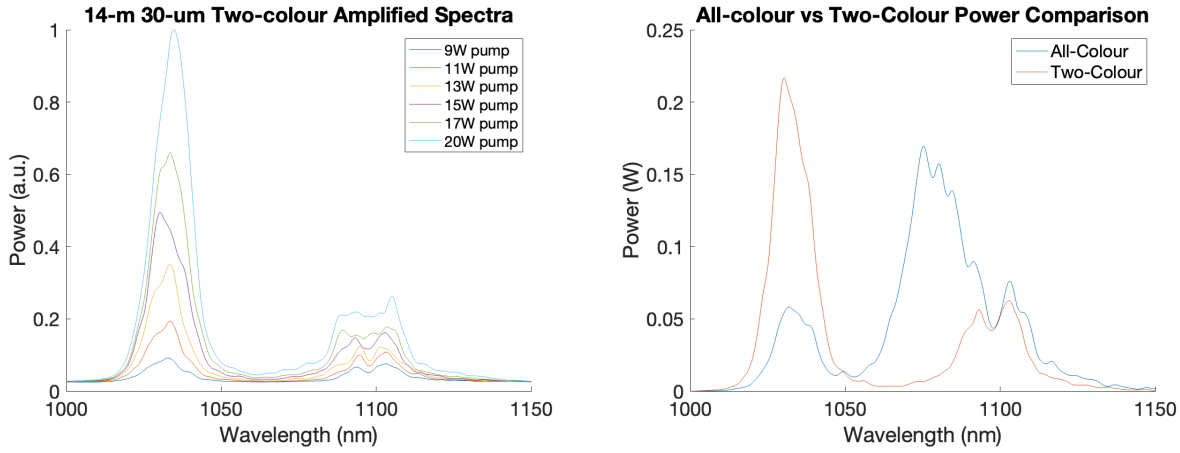

(a) (b)

Figure 4.13: 14-m 30-μm core Yb fiber spliced to combiner along with 975-nm laser diode for counter-pumping. Figure shows amplification of two-colour input with colours at 1030 nm and 1100 nm (a) and a power comparison of the amplified two-colour spectrum and the amplified all-colour spectrum.

The resulting amplified two-colour spectrum is a strong result, with the two-colours having a total power of 7.5 W at 20 W of pump power. This corresponds to a pulse energy of 776 nJ. The blue and red colours have a 17-nm and 21-nm bandwidth respectively. In order to determine whether the pump was making it through the gain fiber, a dichroic mirror was placed at the input end of the gain fiber which transmits wavelengths at 975-nm. At 7 Watts of counterpump, we measured 4 mW of 975-nm light coming through the dichroic, implying that the pump light was making it through the entirety of the fiber. The characteristics of the blue colour are not the same as with the 20-m fiber experimental setup where we saw the amplified ASE amplifying and filling in the gap. Here, we do not see the blue colour exhibiting broadening but it does look like the nonlinear effects are balancing the gain narrowing as the two-colours are retaining their bandwidth. This is a clear advantage of the two-colour nonlinear amplifier setup when comparing to a two-colour CPA setup which would inevitably experience gain narrowing.

According to equation 3.3, the generated MIR power from difference frequency gener-

ation is directly proportional to the product of the two wavelengths being mixed in the nonlinear crystal. We want to determine whether cutting out the central wavelengths of our spectrum results in higher power at the outer wavelengths after amplification when compared to simply amplifying the entire GMNA spectrum as this would determine whether the two-colour amplification would eventually result in higher power MIR. The power comparison between the two-colour amplification and the all-colour amplification can be seen in figure 4.13b. The amplified all-colour spectrum displays a peculiar absorption around 1050-nm which was determined to only be present upon passing through the Yb-fiber and not an unwanted absorption from an optical component preceding the fiber. It also displays a strong gain peak at 1080-nm. When comparing the power at the outer wavelengths for the two-colour vs all-colour amplification, we see that the red wavelengths are nearly identical while the blue wavelengths are 3.75 times more powerful when amplifying the two-colour seed.

As previously discussed in the chapter on mid-infrared generation, conservation of energy tells us that $\omega_i = \omega_p - \omega_s$ for the process of difference frequency generation. In our two-colour laser, the blue colour acts as ω_p and the red colour serves as ω_s. We can determine which wavelengths we would potentially be able to generate by putting this in terms of wavelength, $1/\lambda_i = 1/\lambda_p - 1/\lambda_s$, where λ_i corresponds to the generated MIR. If we consider the outermost wavelengths, 1027 nm and 1109 nm, the corresponding difference frequency generated wavelength would be 13.9 μm. If we consider the inner most wavelengths of our generated two-colour spectrum, 1041 nm and 1085 nm, the corresponding DFG wavelength would be 25.7 μm. However, GaSe crystals are limited by their transparency for wavelengths past 20 μm, meaning that we need a minimum of 55 nm separation between colours to generate MIR. Therefore, this amplified two-colour spectrum could potentially generate MIR tunable from 13.9 - 20 μm.

4.3.2.3 14-m Yb Fiber Two-Colour Amplification using Linear Polarization maintaining GMNA Output

As discussed in section 4.2, a new GMNA output was obtained upon changing the ANDi's output isolator and fixing the grating compressor before the GMNA. This new output emitted similar power levels but retained its linear polarization which meant that we would now be able to able to send linearly polarized light into the two-colour fiber amplifier. The polarization maintaining Yb-doped fiber would then be able to emit linearly polarized light after amplification of the two-colours and allow for efficient compression using diffraction gratings in preparation for difference frequency generation.

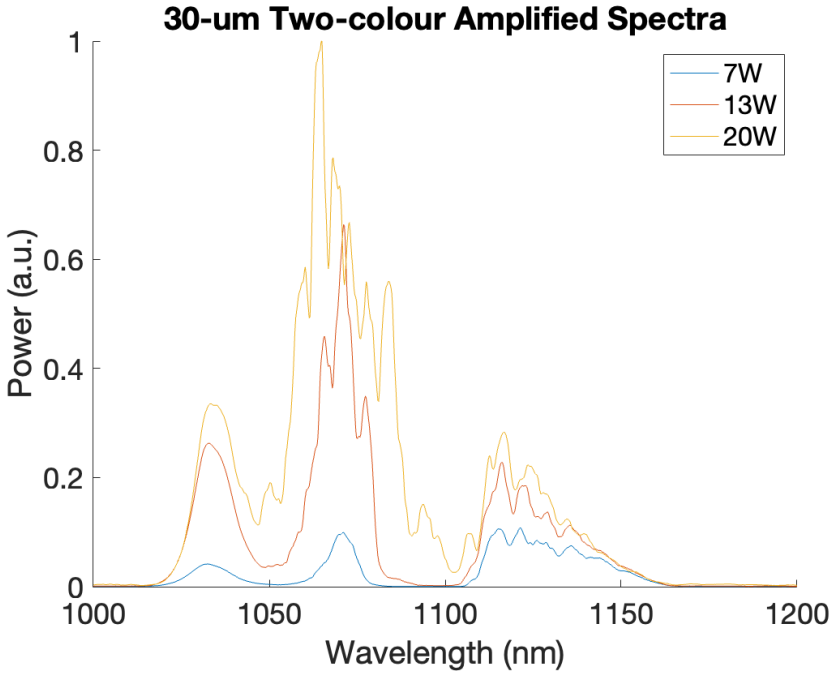

Figure 4.14: Amplification of two colour spectra in 14-m of 30-μm core Yb fiber using polarization maintaining output of GMNA as seed.

Other than the new GMNA output, the same experimental setup was used as in section 4.3.2.2. The notch filter was adjusted to achieve an optimal two-colour seed spectrum which

resulted in blue and red colours centered at 1070-nm and 1120-nm respectively. The blue colour displayed obvious signs of broadening with a bandwidth of 30-nm being achieved with 20 Watts of counter-pump, as seen in figure 4.14. The red colour did not display the same broadening but maintained a bandwidth of 21-nm. We did observe ASE building on the blue side of the spectrum at 1030-nm. The total power of the amplified two-colour spectrum was 6.76-W at 20 Watts of counter-pump, with a total pulse energy of 700 nJ, where the parasitic amplification of spontaneous emission must also be taken into account.

Once again, we can consider what the potential wavelengths of the generated MIR could be, based on this two-colour spectrum, through $1/\lambda_i = 1/\lambda_p - 1/\lambda_s$. The outermost wavelengths, 1056 nm and 1135 nm, correspond to a generated MIR wavelength of 15.2 μm. This two-colour spectrum could potentially generate MIR tunable from 15.2 - 20 μm, limited by the transparency of the GaSe crystal at 20 μm.

Chapter 5

Conclusion

This thesis focused on the development of a nonlinearly amplified two-colour laser system which could be used for the generation of a tunable MIR source through difference frequency generation. We implemented an all-normal dispersion fiber laser in combination with a gain-managed nonlinear amplifier to emit 120-nm 6-ps pulses at a 9.7 MHz repetition rate from which we could select the two colours. After experimenting with various two-colour selection and amplification setups, we determined that our pulse energy was too high for the 10-micron core Yb:fiber as the nonlinear effects caused the gap between the two colours to completely fill in and even created new wavelengths on the red side of the spectrum through noise-induced Raman scattering. We implemented a large-mode-area 30-micron core fiber in order to reduce optical intensities inside the fiber, which yielded much better results. The strongest results were achieved upon selecting the two-colours with a notch filter, and counterpumping the Yb:fiber with up to 20 W of power. The blue and red colours were centered at 1070-nm and 1120-nm with bandwidths of 30-nm and 21-nm being achieved respectively. These broad colours demonstrate the advantage of nonlinear amplification as the nonlinear effects compensate for the gain narrowing that would occur under a two-colour CPA system. This two-colour spectrum could potentially generate mid-infrared that is tunable from 15.2 - 20 μm. The total output power of the

two-colour system was 6.76 W, corresponding to a total pulse energy of 700 nJ, which included significant ASE power around 1030 nm.

Future research could work to reduce the ASE in this system by providing conditions which would allow the blue input seed to outcompete the ASE at these wavelengths. This could potentially be done by shortening the gain fiber. If this ASE is mitigated and the blue input seed is amplified at wavelengths around 1030 nm, a wavelength separation of over 100-nm could be achieved. This could correspond to MIR wavelengths around 11 μm which, after frequency doubling, would allow nearly the entirety of the molecular fingerprint region to be covered by this two-colour source. Further work could be done on studying the energy of the two-colour input and how it affects the output spectrum. By including an efficient compressor, one could study how different pulse durations affect the broadening in the nonlinearly amplified two-colour output.

References

[1] Rudiger Paschotta, Johan Nilsson, Anne C Tropper, and David C Hanna. Ytterbium-doped fiber amplifiers. *IEEE Journal of quantum electronics*, 33(7):1049–1056, 1997.

[2] Konstantin L Vodopyanov. *Laser-based mid-infrared sources and applications*. John Wiley & Sons, 2020.

[3] Daniel Popa and Florin Udrea. Towards integrated mid-infrared gas sensors. *Sensors*, 19(9):2076, 2019.

[4] Bobby Pejcic, Matthew Myers, and Andrew Ross. Mid-infrared sensing of organic pollutants in aqueous environments. *Sensors*, 9(8):6232–6253, 2009.

[5] Angela B Seddon. Mid-infrared (IR)–a hot topic: The potential for using mid-IR light for non-invasive early detection of skin cancer in vivo. *physica status solidi (b)*, 250(5):1020–1027, 2013.

[6] Ting Wang and Luis E Rodriguez-Saona. Rapid determination of sugar level in snack products using infrared spectroscopy. *Journal of food science*, 77(8):C874–C879, 2012.

[7] Robert E Miles, X-C Zhang, Heribert Eisele, and Arunas Krotkus. Terahertz frequency detection and identification of materials and objects. *Springer Science & Business Media*, 2007.

[8] Pavel Sidorenko, Walter Fu, and Frank Wise. Nonlinear ultrafast fiber amplifiers beyond the gain-narrowing limit. *Optica*, 6(10):1328–1333, 2019.

[9] HW Etzel, HW Gandy, and RJ Ginther. Stimulated emission of infrared radiation from ytterbium activated silicate glass. *Applied Optics*, 1(4):534–536, 1962.

[10] DC Hanna, RM Percival, IR Perry, AC Tropper, and JE Townsend. Continuous-wave oscillation of a monomode ytterbium doped fibre laser. 1988.

[11] JR Buckley, SW Clark, and FW Wise. Generation of ten-cycle pulses from an ytterbium fiber laser with cubic phase compensation. *Optics Letters*, 31(9):1340–1342, 2006.

[12] Xiangyu Zhou, Dai Yoshitomi, Yohei Kobayashi, and Kenji Torizuka. Generation of 28-fs pulses from a mode-locked ytterbium fiber oscillator. *Optics Express*, 16(10):7055–7059, 2008.

[13] Yang Lan, Youjian Song, Minglie Hu, Bowen Liu, Lu Chai, and Chingyue Wang. Enhanced spectral breathing for sub-25 fs pulse generation in a yb-fiber laser. *Optics Letters*, 38(8):1292–1294, 2013.

[14] Takashi Kurita, Hidetsugu Yoshida, Toshiyuki Kawashima, and Noriaki Miyanaga. Generation of sub-7-cycle optical pulses from a mode-locked ytterbium-doped single-mode fiber oscillator pumped by polarization-combined 915 nm laser diodes. *Optics Letters*, 37(19):3972–3974, 2012.

[15] Michael Müller, Christopher Aleshire, Arno Klenke, Elissa Haddad, François Légaré, Andreas Tünnermann, and Jens Limpert. 10.4 kW coherently combined ultrafast fiber laser. *Optics Letters*, 45(11):3083–3086, 2020.

[16] Henning Stark, Joachim Buldt, Michael Müller, Arno Klenke, and Jens Limpert. 1 kW, 10 mJ, 120 fs coherently combined fiber CPA laser system. *Optics Letters*, 46(5):969–972, 2021.

[17] EA Shcherbakov, VV Fomin, AA Abramov, AA Ferin, DV Mochalov, and Valentin P Gapontsev. Industrial grade 100 kW power CW fiber laser. In *Advanced Solid State Lasers*. Optica Publishing Group, 2013.

[18] Jiapo Sun, Lie Liu, Lianghua Han, Qixin Zhu, Xiang Shen, and Ke Yang. 100 kW ultra high power fiber laser. *Optics Continuum*, 1(9):1932–1938, 2022.

[19] Jens Limpert, Fabian Roser, Thomas Schreiber, and AJIJ Tunnermann. High-power ultrafast fiber laser systems. *IEEE Journal of selected topics in Quantum Electronics*, 12(2):233–244, 2006.

[20] Andreas Tünnermann, Thomas Schreiber, and Jens Limpert. Fiber lasers and amplifiers: an ultrafast performance evolution. *Applied Optics*, 49(25):F71–F78, 2010.

[21] Dongfeng Liu, Jie Song, and Donna Strickland. Dual-wavelength ultrashort Yb: fiber amplifier. In *Photonics North 2004: Photonic Applications in Telecommunications, Sensors, Software, and Lasers*, volume 5579, pages 744–749. SPIE, 2004.

[22] R Romero-Alvarez, R Pettus, Z Wu, and D Strickland. Two-color fiber amplifier for short-pulse, mid-infrared generation. *Optics Letters*, 33(10):1065–1067, 2008.

[23] AM Al-Kadry and D Strickland. Generation of 400 μW at 17.5 μm using a two-color Yb fiber chirped pulse amplifier. *Optics Letters*, 36(7):1080–1082, 2011.

[24] Xinyang Su, Tuyen Hoang, Pin Long, Yi Zheng, and Donna Strickland. A compact high-average-power femtosecond fiber-coupled two-color cpa system. *IEEE Journal of Selected Topics in Quantum Electronics*, 24(5):1–5, 2018.

[25] A.J. Budz, J. Waisman, H.F. Tiedje, and H.K. Haugen. Short-pulse dual-wavelength system based on mode-locked diode lasers with a single polarization-maintaining Yb: fiber amplifier. *Journal of Lightwave Technology*, 27(16):3416–3424, 2009.

[26] Yangbo Bai, Wanghua Xiang, Peng Zu, and Guizhong Zhang. Tunable dual-wavelength passively mode-locked Yb-doped fiber laser using SESAM. *Chinese Optics Letters*, 10(11):111405–111405, 2012.

[27] Xiaojun Zhu, Wen Liu, Yongquan Pan, Shuai Li, Guoan Zhang, Yancheng Ji, Li Zou, Zhipeng Liang, and Juan Cao. Tunable dual-wavelength with twin-pulse dissipative solitons in all-normal dispersion Yb-doped fiber laser. *Micromachines*, 13(7):1049, 2022.

[28] Walter Koechner. *Solid-state laser engineering*, volume 1. Springer, 2013.

[29] Moulton. Spectroscopic and laser characteristics of Ti:Al_2O_3. *SPIE Milestone Series*, (173):327–335, 2002.

[30] Burns Sibbett Evans, Spence. Dual-wavelength self-mode-locked Ti:sapphire laser. *Optics Letters*, 18(13):1074–1076, 1993.

[31] Laubereau Leitenstorfer, Fürst. Widely tunable two-color mode-locked Ti: sapphire laser with pulse jitter of less than 2 fs. *Optics Letters*, 20(8):916–918, 1995.

[32] Zhuhong Zhang, Adam M. Deslauriers, and Donna Strickland. Dual-wavelength chirped-pulse amplification system. *Optics Letters*, 25(8):581–583, 2000.

[33] Strickland Xia, Song. Development of a dual-wavelength Ti:sapphire multi-pass amplifier and its application to intense mid-infrared generation. *Optics Communications*, 206(1-3):149–157, 2002.

[34] Legare Villeneuve Likforman Joffre Corkum Fraser, Cheung. High-energy sub-picosecond pulse generation from 3 to 20 μm. *Applied Physics B*, 74:s153–s156, 2002.

[35] Koichi Yamakawa and C.P.J. Barty. Two-color chirped-pulse amplification in an ultra-broadband Ti:sapphire ring regenerative amplifier. *Optics letters*, 28(23):2402–2404, 2003.

[36] Koichi Yamakawa and Christopher P.J. Barty. Ultrafast, ultrahigh-peak, and high-average power Ti:sapphire laser system and its applications. *IEEE Journal of Selected Topics in Quantum Electronics*, 6(4):658–675, 2000.

[37] Govind P Agrawal. Nonlinear fiber optics. In *Nonlinear Science at the Dawn of the 21st Century*, pages 195–211. Springer, 2000.

[38] Robert W Boyd, Alexander L Gaeta, and Enno Giese. Nonlinear optics. In *Springer Handbook of Atomic, Molecular, and Optical Physics*, pages 1097–1110. Springer, 2008.

[39] Ursula Keller and R Paschotta. *Ultrafast Lasers*. Springer, 2021.

[40] Donna Strickland and Gerard Mourou. Compression of amplified chirped optical pulses. *Optics Communications*, 55(6):447–449, 1985.

[41] Wei Zhao, Xiaohong Hu, and Yishan Wang. Femtosecond-pulse fiber based amplification techniques and their applications. *IEEE Journal of Selected Topics in Quantum Electronics*, 20(5):512–524, 2014.

[42] Yoann Zaouter, Dimitris N Papadopoulos, Marc Hanna, J Boullet, L Huang, Claude Aguergaray, Frédéric Druon, Eric Mottay, Patrick Georges, and Eric Cormier. Stretcher-free high energy nonlinear amplification of femtosecond pulses in rod-type fibers. *Optics Letters*, 33(2):107–109, 2008.

[43] Wei Liu, Damian N Schimpf, Tino Eidam, Jens Limpert, Andreas Tünnermann, Franz X Kärtner, and Guoqing Chang. Pre-chirp managed nonlinear amplification in fibers delivering 100 W, 60 fs pulses. *Optics Letters*, 40(2):151–154, 2015.

[44] Martin E Fermann, VI Kruglov, BC Thomsen, John M Dudley, and John D Harvey. Self-similar propagation and amplification of parabolic pulses in optical fibers. *Physical Review Letters*, 84(26):6010, 2000.

[45] Daniel B Soh, Johan Nilsson, and Anatoly B Grudinin. Efficient femtosecond pulse generation using a parabolic amplifier combined with a pulse compressor. ii. finite gain-bandwidth effect. *JOSA B*, 23(1):10–19, 2006.

[46] Pavel Sidorenko, Walter Fu, and Frank W Wise. Gain-managed nonlinear fiber amplifier. In *The European Conference on Lasers and Electro-Optics*. Optica Publishing Group, 2019.

[47] Pavel Sidorenko and Frank Wise. Generation of 1 μJ and 40 fs pulses from a large mode area gain-managed nonlinear amplifier. *Optics Letters*, 45(14):4084–4087, 2020.

[48] Ying Han, Yubin Guo, Bo Gao, Chunyang Ma, Ruohan Zhang, and Han Zhang. Generation, optimization, and application of ultrashort femtosecond pulse in mode-locked fiber lasers. *Progress in Quantum Electronics*, 71:100264, 2020.

[49] Fermann. Nonlinear polarization evolution in passively modelocked fiber lasers. *Cambridge Studies in Modern Optics*, pages 179–179, 1995.

[50] Heng Li, Dimitre G Ouzounov, and Frank W Wise. Starting dynamics of dissipative-soliton fiber laser. *Optics Letters*, 35(14):2403–2405, 2010.

[51] Brandon G Bale, J Nathan Kutz, Andy Chong, William H Renninger, and Frank W Wise. Spectral filtering for mode locking in the normal dispersive regime. *Optics Letters*, 33(9):941–943, 2008.

[52] Andy Chong, Joel Buckley, Will Renninger, and Frank Wise. All-normal-dispersion femtosecond fiber laser. *Optics Express*, 14(21):10095–10100, 2006.

[53] Andy Chong, William H Renninger, and Frank W Wise. All-normal-dispersion femtosecond fiber laser with pulse energy above 20 nJ. *Optics Letters*, 32(16):2408–2410, 2007.

[54] Robert W Boyd. *Nonlinear optics*. Academic press, 2020.

[55] Qian Cao, Franz X Kärtner, and Guoqing Chang. Towards high power longwave mid-IR frequency combs: power scalability of high repetition-rate difference-frequency generation. *Optics Express*, 28(2):1369–1384, 2020.

[56] JE Midwinter and J Warner. The effects of phase matching method and of uniaxial crystal symmetry on the polar distribution of second-order non-linear optical polarization. *British Journal of Applied Physics*, 16(8):1135, 1965.

[57] Giulio Cerullo and Sandro De Silvestri. Ultrafast optical parametric amplifiers. *Review of Scientific Instruments*, 74(1):1–18, 2003.

[58] Luke Maidment, Oguzhan Kara, Peter G Schunemann, Jonathon Piper, Kenneth McEwan, and Derryck T Reid. Long-wave infrared generation from femtosecond and picosecond optical parametric oscillators based on orientation-patterned gallium phosphide. *Applied Physics B*, 124(7):1–8, 2018.

[59] Marcus Beutler, Ingo Rimke, Edlef Büttner, Paolo Farinello, Antonio Agnesi, Valeriy Badikov, Dmitrii Badikov, and Valentin Petrov. Difference-frequency generation of ultrashort pulses in the mid-IR using yb-fiber pump systems and $AgGaSe_2$. *Optics Express*, 23(3):2730–2736, 2015.

[60] Tobias Steinle, Florian Mörz, Andy Steinmann, and Harald Giessen. Ultra-stable high average power femtosecond laser system tunable from 1.33 to 20 μm. *Optics Letters*, 41(21):4863–4866, 2016.

[61] Miriam RX de Barros, Rubens S Miranda, Tom M Jedju, and Philippe C Becker. High-repetition-rate femtosecond mid-infrared pulse generation. *Optics Letters*, 20(5):480–482, 1995.

[62] S Ehret and H Schneider. Generation of subpicosecond infrared pulses tunable between 5.2 μm and 18 μm at a repetition rate of 76 MHz. *Applied Physics B: Lasers & Optics*, 66(1), 1998.

[63] J Song, JF Xia, Z Zhang, and D Strickland. Mid-infrared pulses generated from the mixing output of an amplified, dual-wavelength Ti:sapphire system. *Optics Letters*, 27(3):200–202, 2002.

[64] Gengji Zhou, Qian Cao, Franz X Kärtner, and Guoqing Chang. Energy scalable, offset-free ultrafast mid-infrared source harnessing self-phase-modulation-enabled spectral selection. *Optics Letters*, 43(12):2953–2956, 2018.

[65] Jarosław Sotor, Tadeusz Martynkien, Peter G Schunemann, Paweł Mergo, Lucile Rutkowski, and Grzegorz Soboń. All-fiber mid-infrared source tunable from 6 to 9 μm based on difference frequency generation in OP-GaP crystal. *Optics Express*, 26(9):11756–11763, 2018.

[66] Xinyang Su, Mingjian Lyu, Tuyen Hoang, Zujun Xu, Yi Zheng, and Donna Strickland. Investigation of long wavelength mid-infrared generation in the tight focusing limit. *Optics Express*, 27(18):24945–24952, 2019.

[67] Houkun Liang, Peter Krogen, Zhou Wang, Hyunwook Park, Tobias Kroh, Kevin Zawilski, Peter Schunemann, Jeffrey Moses, Louis F DiMauro, Franz X Kärtner, et al. High-energy mid-infrared sub-cycle pulse synthesis from a parametric amplifier. *Nature Communications*, 8(1):1–9, 2017.

[68] Marcus Seidel, Xiao Xiao, Syed A Hussain, Gunnar Arisholm, Alexander Hartung, Kevin T Zawilski, Peter G Schunemann, Florian Habel, Michael Trubetskov, Vladimir Pervak, et al. Multi-Watt, multi-octave, mid-infrared femtosecond source. *Science Advances*, 4(4), 2018.

[69] U Elu, T Steinle, D Sánchez, L Maidment, K Zawilski, P Schunemann, UD Zeitner, C Simon-Boisson, and J Biegert. Table-top high-energy 7 μm OPCPA and 260 mJ Ho:YLF pump laser. *Optics Letters*, 44(13):3194–3197, 2019.

[70] Abijith S Kowligy, Henry Timmers, Alexander J Lind, Sylvain Karlen, Flavio Cruz, Peter G Schunemann, Jens Biegert, and Scott A Diddams. Near-single-cycle long-

wave infrared pulses for coherent linear and nonlinear optics. In *CLEO: Science and Innovations*. Optica Publishing Group, 2019.

[71] Jinwei Zhang, Ka Fai Mak, Nathalie Nagl, Marcus Seidel, Dominik Bauer, Dirk Sutter, Vladimir Pervak, Ferenc Krausz, and Oleg Pronin. Multi-mW, few-cycle mid-infrared continuum spanning from 500 to 2250 cm^{-1}. *Light: Science & Applications*, 7(2):17180–17180, 2018.

[72] Sida Xing, Daniel MB Lesko, Takeshi Umeki, Alexander J Lind, Nazanin Hoghooghi, Tsung-Han Wu, and Scott A Diddams. Single-cycle all-fiber frequency comb. *APL Photonics*, 6(8):086110, 2021.

[73] Hadil Kassab, Sebastian Gröbmeyer, Wolfgang Schweinberger, Christina Hofer, Philipp Steinleitner, Maximilian Högner, Tatiana Amotchkina, Daniel Gerz, Matthias Knorr, Rupert Huber, et al. In-line synthesis of multi-octave phase-stable infrared light. *Optics Express*, 31(15):24862–24874, 2023.

[74] Kun Liu, Houkun Liang, Shizhen Qu, Wenkai Li, Xiao Zou, Ying Zhang, and Qi Jie Wang. High-energy mid-infrared intrapulse difference-frequency generation with 5.3% conversion efficiency driven at 3 μm. *Optics Express*, 27(26):37706–37713, 2019.

[75] Q Bournet, F Guichard, M Natile, Y Zaouter, M Joffre, A Bonvalet, Ioachim Pupeza, Christina Hofer, F Druon, Marc Hanna, et al. Enhanced intrapulse difference frequency generation in the mid-infrared by a spectrally dependent polarization state. *Optics Letters*, 47(2):261–264, 2022.

[76] Federico Capasso. High-performance midinfrared quantum cascade lasers. *Optical Engineering*, 49(11):111102, 2010.

[77] Jerome Faist, Federico Capasso, Deborah L Sivco, Carlo Sirtori, Albert L Hutchinson, and Alfred Y Cho. Quantum cascade laser. *Science*, 264(5158):553–556, 1994.

[78] Daniel Hofstetter, Mattias Beck, Thierry Aellen, and Jérôme Faist. High-temperature operation of distributed feedback quantum-cascade lasers at 5.3 μm. *Applied Physics Letters*, 78(4):396–398, 2001.

[79] Manijeh Razeghi. High-performance InP-based mid-IR quantum cascade lasers. *IEEE Journal of Selected Topics in Quantum Electronics*, 15(3):941–951, 2009.

[80] Arkadiy Lyakh, Richard Maulini, Alexei Tsekoun, Rowel Go, Christian Pflügl, Laurent Diehl, Qi Jie Wang, Federico Capasso, and C Kumar N Patel. 3 W continuous-wave room temperature single-facet emission from quantum cascade lasers based on nonresonant extraction design approach. *Applied Physics Letters*, 95(14):141113, 2009.

[81] Richard Maulini, Dmitri A Yarekha, Jean-Marc Bulliard, Marcella Giovannini, Jérôme Faist, and Emilio Gini. Continuous-wave operation of a broadly tunable thermoelectrically cooled external cavity quantum-cascade laser. *Optics Letters*, 30(19):2584–2586, 2005.

[82] Andreas Wittmann, Andreas Hugi, E Gini, N Hoyler, and Jérôme Faist. Heterogeneous high-performance quantum-cascade laser sources for broad-band tuning. *IEEE Journal of Quantum Electronics*, 44(11):1083–1088, 2008.

[83] Andreas Hugi, Richard Maulini, and Jérôme Faist. External cavity quantum cascade laser. *Semiconductor Science and Technology*, 25(8):083001, 2010.

[84] N Bandyopadhyay, M Chen, S Sengupta, S Slivken, and M Razeghi. Ultra-broadband quantum cascade laser, tunable over 760 cm^{-1}, with balanced gain. *Optics Express*, 23(16):21159–21164, 2015.